Dissertação de Mestrado

Characterization of axon-Schwann cell interactions implicated in neuronal energy metabolism

Ana Carolina Temporão Marques Filipe

Mestrado Integrado em Bioengenharia – Biotecnologia Molecular

2018

Supervisor

Roman Chrast, PhD

Departamento de Neurociência e Departamento de Neurociência Clínica, Instituto Karolinska, Estocolmo, Suécia

Co-supervisor

Filipa Bouçanova, MSc

Departamento de Neurociência e Departamento de Neurociência Clínica, Instituto Karolinska, Estocolmo, Suécia

Co-supervisor

Joana Paes de Faria, PhD

Instituto de Investigação e Inovação em Saúde, Universidade do Porto, Porto, Portugal

Instituto de Biologia Molecular e Celular, Universidade do Porto, Porto, Portugal

Caracterização de interações axónio-célula de Schwann implicadas no metabolismo de energia neuronal

Characterization of axon-Schwann cell interactions implicated in neuronal energy metabolism

Ana Carolina Temporão Marques Filipe

Supervisor: Doutor Roman Chrast
Co-supervisor: Filipa Bouçanova
Co-supervisor: Doutora Joana Paes de Faria

Faculdade de Engenharia da Universidade do Porto, Portugal
Instituto de Ciências Biomédicas Abel Salazar da Universidade do Porto, Portugal
Instituto Karolinska, Suécia
Instituto de Investigação e Inovação em Saúde, Portugal
Instituto de Biologia Molecular e Celular, Universidade do Porto, Porto, Portugal

Fevereiro 2018

Agradecimentos

Há cinco anos, a semente,
Moldada pelos grãos de uma terra fértil,
Brotava e espreitava curiosa
O encanto da luz do dia.

Penetrando a terra, as raízes revigoravam
E importavam nutrientes da água saciante
Para o caule ascender com empenho e diversão.

E ascendeu.
Cada pedaço de luz absorveu,
E cada instante de vida saboreou.
Primaveras com rebentos,
E verões abrasadores.
Outonos com brisas
E Invernos com nórdicos ventos.

Percurso belo, imortal,
Que agora é saudoso.

Terra, a família.
Água, as amizades.
Luz, o curso.
A todos vós…
Obrigada pela vida.

Eis a flor.
Que venha o fruto.

Author Contributions

Ana Temporão performed the studies of glutamate stimulation in SC cultures; contributed to the initial set up of the FRET-based experiments; characterized the mouse models by genotyping, qPCR and immunohistochemistry; and wrote the manuscript.

Filipa Bouçanova designed research; supervised the studies of glutamate stimulation in SC cultures; performed FRET-based experiments; characterized the mouse models by genotyping, qPCR and immunohistochemistry; and guided the writing of the manuscript.

Roman Chrast designed research, provided intellectual support along the project, and guided the writing of the manuscript.

Joana Paes de Faria guided the writing of the manuscript.

Poster presentations

Filipa Bouçanova, Ana Temporão, Enric Domènech-Estévez, Hasna Baloui, Linnéa Nilsson, Hjalmar Brismar and Roman Chrast. *Characterization of axon-Schwann cell interactions implicated in neuronal energy metabolism.*

- 2nd Biomedicum Young Researchers Symposium (2018; Stockholm, Sweden)
- II Nordic Neuroscience (2017; Stockholm, Sweden)
- StratNeuro Retreat (2017; Stockholm, Sweden)

Resumo

O sistema nervoso periférico (SNP) é composto por nervos sensoriais e motores que, respectivamente, detectam sinais internos ou externos, como dor e calor, e estimulam tecidos efectores como glândulas e músculos para realizar uma função ou reflexo. Um SNP funcional depende inteiramente da integridade da relação entre o axónio e a célula de Schwann (SC), sendo esta essencial para o próprio desenvolvimento e para a manutenção a longo prazo dos nervos periféricos. Assim, a disrupção da comunicação axo-glial pode estar envolvida na patogénese de neuropatias periféricas, como a doença de Charcot-Marie-Tooth, neuropatias diabéticas e esclerose lateral amiotrófica, que apresentam alta prevalência a nível mundial. Por essa razão, é imperativo explorar mais profundamente a fisiologia e a fisiopatologia do SNP, a fim de que novos caminhos terapêuticos se abram para modular a progressão dessas doenças.

Uma potencial nova função das SCs é a de fornecer suporte metabólico e energético ao axónio subjacente. Ambas as células no SNP expressam transportadores de monocarboxilatos (MCTs) através dos quais substratos altamente energéticos, como o lactato, podem ser trocados. Embora a distribuição celular dos diferentes MCTs sugira um tráfego metabólico da SC para o axónio, a sua caracterização funcional é ainda desconhecida. Para além disso, não é claro em que medida o suporte metabólico é necessário. Será continuamente fornecido pela glia ou apenas desencadeado por necessidades energéticas mais elevadas dos axónios, como durante a atividade neuronal?

Para preencher a lacuna existente na área, nós colocamos a hipótese de que as SCs detetam a atividade neuronal via receptores de neurotransmissores, desencadeando cascatas de sinalização intracelular e potencialmente aumentando o importe/a geração de lactato. Este monocarboxilato pode então ser transferido para o axónio através de MCTs para a produção de energia.

Com este trabalho, nós mostrámos que a breve exposição ao glutamato desencadeia a ativação das vias de sinalização ERK e AKT/mTOR/S6RP em culturas primárias de SCs, principalmente quando são previamente expostas a neuregulina-1. Essas respostas intracelulares podem preceder ajustes na sua atividade metabólica. Para avaliar potenciais variações nos níveis de lactato intracelular, começámos a estabelecer um ensaio baseado em FRET usando células HEK293T e uma sonda de deteção de lactato codificada geneticamente, a Laconic. O conhecimento assim obtido será no futuro aplicado a SCs. Finalmente, observámos preliminarmente que a ablação de MCT1 ou MCT4 especificamente em SCs não parece perturbar a estrutura nem a função do SNP, o que pode dever-se a uma expressão compensatória de outros transportadores.

Palavras-chave

Sistema nervoso periférico; Célula de Schwann; Glutamato; Lactato; Transportadores de monocarboxilatos

Abstract

The peripheral nervous system (PNS) is composed of sensory and motor nerves that, respectively, detect internal or external signals such as pain and heat, and stimulate effectors like glands and muscles to perform a function or reflex. A functional PNS relies entirely on the integrity of the axon-Schwann cell (SC) unit and the crosstalk between the two partners is essential for proper development and long-term maintenance of peripheral nerves. Thus, impaired SC-axon communication may be involved in the pathogenesis of peripheral neuropathies, such as Charcot-Marie-Tooth disease, diabetic neuropathies and amyotrophic lateral sclerosis, which show high prevalence worldwide. For that reason, it is imperative to explore more deeply the physiology and pathophysiology of the PNS, so that new therapeutic avenues open to modulate the progression of these diseases.

One potential novel role of SCs is to provide metabolic and energetic support to the underlying axon. Both cells in the PNS express monocarboxylate transporters (MCTs) through which high energetic substrates, such as lactate, can be exchanged. Although the cellular distribution of different MCTs suggests SC-to-axon metabolic traffic, their functional characterization is still missing. Furthermore, it is not clear to what extent metabolic support is required. Is it continuously provided by glia or only triggered by higher energy demands of axons, such as during neuronal activity?

To fill the existing gap in the field, we hypothesized that SCs detect neuronal activity via receptors for neurotransmitters, triggering intracellular signaling cascades and potentially increasing lactate import/generation. This monocarboxylate may then be transferred to the axon through MCTs for energy production.

Here, we show that short exposure to glutamate triggers the activation of ERK and AKT/mTOR/S6RP signaling pathways in primary cultured SCs, particularly when primed with neuregulin-1. These intracellular response may precede adjustments in their metabolic activity. To evaluate potential variations in intracellular lactate levels, we started to establish a FRET-based assay using HEK293T cells and a genetically encoded lactate-sensing probe, Laconic. The knowledge obtained with this will be applied to SCs in the future. Finally, we preliminarily observed that SC-specific ablation of either MCT1 or MCT4 does not seem to perturb PNS structure and function, which could be due to a compensatory expression of other transporters.

Keywords

Peripheral nervous system; Schwann cell; Glutamate; Lactate; Monocarboxylate transporter

Abbreviations List

AKT – Protein kinase B
ALS – Amyotrophic lateral sclerosis
AMPA – α-amino-3-hydroxy-5-methyl-4-isoxazolepropionic acid
ANLSH – Astrocyte-neuron lactate shuttle hypothesis
ARC – AR-C155858
ATP – Adenosine triphosphate
BCA – Bicinchoninic acid assay
BPE – Bovine pituitary extract
BSA – Bovine serum albumin
cKO – Conditional knockout
CMT – Charcot-Marie-Tooth diseases
CNS – Central nervous system
DAPI – 4',6-diamidino-2-phenylindole, dihydrochloride
DMEM – Dulbecco's modified eagle medium
DNA – Deoxyribonucleic acid
DRG – Dorsal root ganglion
ECL – Enhanced chemiluminescence
EDL – Extensor digitalis longus
EDTA – Ethylenediamine tetraacetic acid
EGF – Epidermal growth factor
ErbB – Epidermal growth factor receptor
ERK – Extracellular signal-regulated kinase
FBS – Fetal bovine serum
FRET – Förster resonance energy transfer
Fsk – Forskolin
Glu – Glutamate
GLUT – Glucose transporter
HEK293T – Human embryonic kidney 293 T cell line
HEPES – 4-(2-hydroxyethyl)-1-piperazineethanesulfonic acid
IENFD – Intraepidermal nerve fiber density
K_D – Dissociation constant
KRH – Krebs-Ringer-HEPES buffer
LDH – Lactate dehydrogenase
LKB1 – Liver kinase B1
MAG – Myelin-associated glycoprotein
MBP – Myelin basic protein
MCT – Monocarboxylate transporter
mGluR – Metabotropic glutamate receptors

MPZ/P0 – Myelin protein zero
mTFP – Monomeric teal fluorescent protein
mTOR – Mammalian target of rapamycin
NGS – Normal goat serum
NMDA – N-methyl-D-aspartic acid
NMDA-R – N-methyl-D-aspartic acid receptor
NMJ – Neuromuscular junction
Nrg1 – Neuroregulin-1
OCT – Optimal cutting temperature
PB – Phosphate buffer
PBS – Phosphate-buffered saline
pCMBS – 4-(Chloromercuri)benzenesulfonic acid sodium salt
PCR – Polymerase chain reaction
PFA – Paraformaldehyde
PGP9.5 – Protein gene product 9.5
PI3K – Phosphoinositide 3-kinase
PLL – Poly-L-Lysine
PLP – Proteolipid protein
Pmp2 – Peripheral myelin protein 2
PNS – Peripheral nervous system
qPCR – Quantitative polymerase chain reaction
RNA – Ribonucleic acid
RT – Room temperature
RT-qPCR – Quantitative real-time polymerase chain reaction
S6RP – S6 ribosomal protein
SC – Schwann cell
SDS – Sodium dodecyl sulphate
PAGE – Polyacrylamide gel electrophoresis
shRNA – Short hairpin RNA
SLI – Schmidt-Lanterman incisure
SN – Sciatic nerve
SOD1 – Superoxide dismutase 1
TBS – Tris-buffered saline
TCA – Tricarboxylic acid
TESPA – 3-triethoxysilylpropylamine
Ubiq – Ubiquitin-conjugating enzyme E2
WB – Western Blot

Table of Contents

1. Introduction

1.1. Peripheral Nervous System: Function, Structure and Development

The peripheral nervous system (PNS) contains all the nerves and ganglia that lie outside the brain and spinal cord, structures that constitute the central nervous system (CNS). While neuronal cell bodies reside within the CNS or the peripheral ganglia, the axons bundle together to build up the nerves. Some of them are composed by sensory fibers, which transmit to the CNS signals from the internal or external environment that are detected by sensory receptors (e.g. mechanoreceptors in the skin). After being processed in the CNS, the output is carried by motor neurons to produce a response upon activation of effector organs, such as muscles and glands. Therefore, the PNS functions as the bond between the CNS and the periphery of the body (Kandel, Schwartz & Jessel, 2000).

Peripheral nerves are organized in a way that three tissue compartments can be distinguished (**Figure 1**). Endoneurium is the innermost part, consisting of connective tissue found between individual axons within a fascicle. Bundles of multiple axons are surrounded by a sheath of fibroblasts and collagenous connective tissue, called perineurium, which functions as a blood-nerve barrier. The epineurium embeds these structures in a collagenous matrix where adipose tissue, elastin fibers and vascular endothelial cells can also be found (Jessen & Mirsky, 1999).

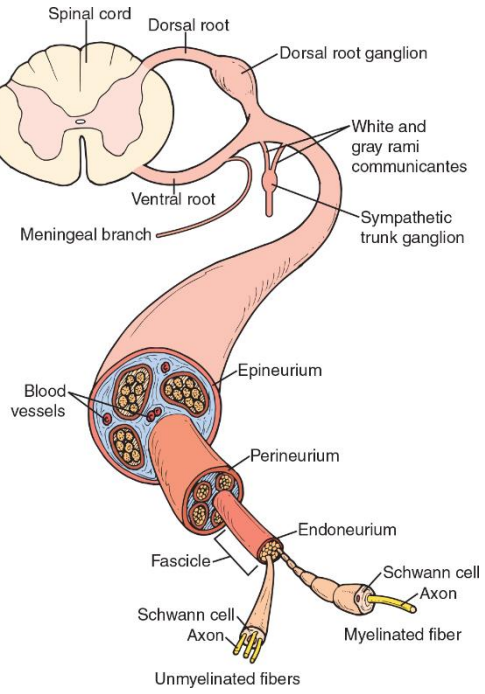

Figure 1. Schematic representation of the structure of peripheral nerves. As found in (Kisner & Colby, 2012)

The structure and function of peripheral nerves is ensured by the intimate interactions established between neurons and glial cells. During development, both cell types derive from the neural plate, which is later divided into neural tube and neural crest. The former differentiates into the brain and spinal cord and into the motor neurons of the PNS. Neural crest cells, in turn, migrate away to the periphery to give rise to all sensory neurons and glial cells of the PNS (Jessen & Mirsky, 2005).

Schwann cells (SCs) are the major type of peripheral glial cells and the counterpart of the oligodendrocytes in the CNS. Both cells spirally extend their cell membrane to produce myelin around axons, even though this process is differently regulated. Besides SCs, peripheral glial cells include satellite cells enveloping cell bodies in the ganglia; perisynaptic SCs at neuromuscular junctions; terminal SCs at sensory axons; olfactory ensheathing cells engulfing axons of the olfactory nerve; and enteric glial cells surrounding autonomic ganglia of the gut (Jessen, 2004).

In the PNS, the maturation of neural crest cells generates SC precursors – found at the embryonic day (E) 12/13 in mouse nerves (Jessen & Mirsky, 2005). Their differentiation around E13-15 in mice gives rise to immature SCs, which are found ensheathing numerous axons of mixed caliber. A fate decision point is reached perinatally, in which immature SCs undergo a morphogenetic process known as radial sorting that leads to the formation of myelinating and non-myelinating SC that ensheath large and small diameter axons, respectively (Feltri et al., 2016).

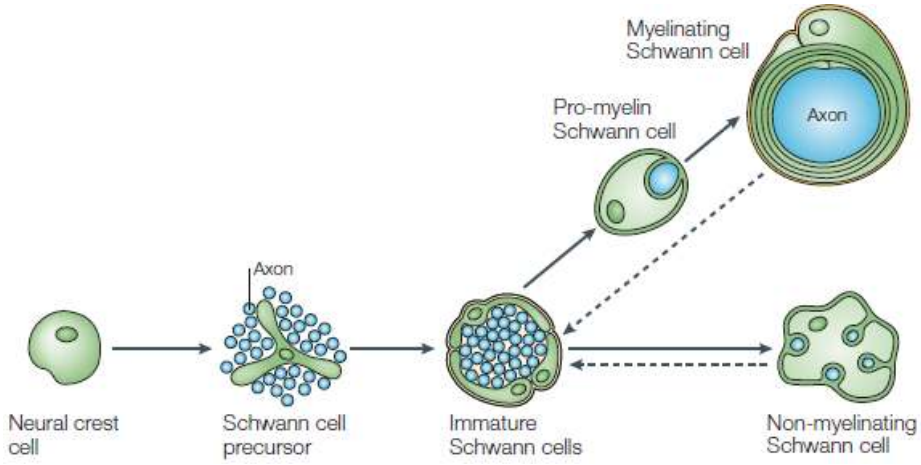

Figure 2 – Schematic representation of the progression of Schwann cell lineage. As found in (Jessen & Mirsky, 2005).

At the moment of decision between myelinating versus non-myelinating phenotype, SC metabolism and gene expression are tightly modulated, in particular by the axons with which they are associated. Among several neuronal growth factors, neuroregulin-1 (Nrg1) plays a major role at this stage of development, instructing the survival, migration, proliferation and differentiation of SC-lineage cells (Nave & Salzer, 2006). This occurs through the signaling of Nrg1 type III via ErbB2/ErbB3 receptors on the glial membrane, which triggers SC's intracellular pathways that

target, among others, ERK and AKT (Harrisingh et al., 2004; Lyons et al., 2005; Ogata et al., 2004).

Thinner axons (diameter < 1µm), which display less Nrg1 at their surface, are ensheathed together by the cytoplasm of non-myelinating SCs into Remak bundles (Griffin & Thompson, 2008; Sherman & Brophy, 2005). Since ion channels are diffusely distributed along the unmyelinated fibers, the signal transmission in Remak bundles is continuous and slow. In large caliber axons (diameter > 1µm), in turn, Nrg1 acts as a positive regulator of myelin-sheath thickness in function of axon size (Michailov et al., 2004). Each axonal segment is then enwrapped by myelin sheath provided by a single myelinating Schwann cell (Feltri, Poitelon, & Previtali, 2016). Interestingly, Nrg1 overexpression in neurons instructs non-myelinating SCs to myelinate *de novo* the thin axons with which they are associated (Taveggia et al., 2005).

Moreover, a notable feature of the PNS is that fully differentiated SCs retain plasticity throughout life and can readily revert to a phenotype similar to that of immature Schwann cells, a phenomenon that typically occurs in response to nerve injury (Ceci et al., 2014; Morrison et al., 1999). Nrg1 also appears to promote SC de-differentiation in injured nerves (Zanazzi et al., 2001).

Although solving similar tasks, the maturation of Schwann cells and oligodendrocytes is distinct and modulated by different factors (Nave & Werner, 2014). Indeed, Nrg1/ErbB signaling is not necessary for CNS myelination to occur and oligodendrocytes only require physical association with axons at the last step of maturation (Brinkmann et al., 2008). Therefore, the regulation of myelination by neurons seems to be less pronounced in the CNS.

There are also clear differences between the CNS and the PNS with respect to the composition of myelin. The most abundant proteins of peripheral myelin are the specific glycoproteins myelin protein zero (MPZ/P0) and protein 2 (Pmp2), whereas CNS myelin is rich in proteolipid protein (PLP) (Jahn et al., 2009; Patzig et al., 2011). Moreover, MBP is not required for PNS myelination but is rate limiting for CNS myelination (Kirschner & Ganser, 1980; Readhead et al., 1987).

Myelin produced by either SCs or oligodendrocytes is repeatedly wrapped and compacted around segments of axons to electrically insulate them (Hildebrand et al., 1993; Webster, 1971). During myelination, the cytoplasmic leaflets of the glial membrane are fused together forming dark dense lines visible in electron microscopy, which alternate with intraperiod lines of the myelin sheath (Scherer & Arroyo, 2002). Nodes of Ranvier consist of the short regions that separate consecutive myelinated segments (internodes) and where action potentials are generated (Salzer, 2003). This way, myelination provides the basis for the rapid and energy efficient saltatory impulse propagation required for motor, sensory, and cognitive functions of the vertebrate nervous system (Nave & Werner, 2014).

To efficiently support this role, axons and glia form a symbiotic unit where distinct structural domains are organized (Salzer, 2003) (**Figure 3**). At each end of the internode, a paranodal junction separates the nodes of Ranvier from a juxtaparanodal region, where Na^+ channels and K^+ channels are respectively clustered (Buttermore et al., 2013). A continuous network of non-compact myelin connects the outermost (abaxonal) region of the myelin sheath,

where most glial organelles and cytosolic components are found, to the innermost (adaxonal) layer, which is in direct contact with the narrow periaxonal space that separates axons from the myelin sheath (Nave, 2010b). This channel-like system is additionally shaped by Cajal bands, positioned underneath the SC plasma membrane, and by the lumina of the paranodal loops and Schmidt-Lanterman incisures, both comprising gap-junction connections between adjacent membranes (Nave, 2010b). SLIs are exclusive structures of the PNS, consisting on local stacks of non-compacted myelin radially disposed around the axon (Nave, 2010b). Hence, although axons are almost completely surrounded by myelin, the intercellular exchange of nutrients, ions and other small molecules can take place in this system of non-compacted myelin that connects the periaxonal space to the glial soma (Nave, 2010b). However, the physiological purposes for the existence of this structure are not completely understood.

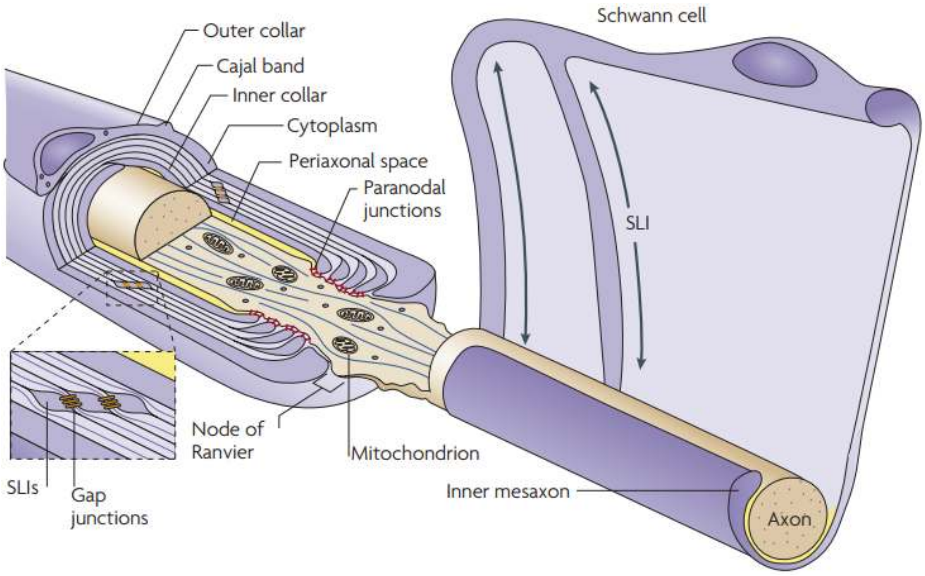

Figure 3 – Schematic representation of a myelinated axon – with the unrolled sheath of SC shown on the right, where several compartments can be distinguished. As found in (Nave, 2010b).

Despite myelination playing a valuable role on the proper function of the vertebrate nervous system, the significance of neuron-glia interactions goes much beyond the benefits provided by myelination itself. Indeed, glial cells also play a critical role on the survival, function and regeneration of neurons, as they regulate their structural integrity, provide trophic and metabolic support, and confer neuroprotection (Samara et al., 2013).

1.2. Metabolic communication between SCs and peripheral axons

The complex functions and large dimension of the nervous system require fast neuronal communication. In vertebrates that is possible by means of myelination, which allows quick and efficient impulse propagation as areas of regeneration of action potentials are restricted to very short regions on the axonal surface (Nave, 2010a). However, myelination itself creates a nearly complete physical barrier that deprives axons from the free access to extracellular metabolites (Nave, 2010b). Nodal uptake of metabolites might not be sufficient to meet their energy demands, at least in fibers with longer internodes, larger caliber, or higher firing frequencies (Hirrlinger & Nave, 2014).

Axons can connect the neuronal cell body to target cells so far away that more than 99% of the neuronal mass is axonal, as it is the case for sciatic nerve fibers (Nave, 2010b). The length and volume of neurons are often further increased by axonal ramifications (Matsuda et al., 2009). Consequently, distal regions of long axons receive limited metabolic resources from the neuronal soma, thus requiring the exchange of metabolites with the surrounding space (Nave, 2010b). Indeed, the assumption that long axons may require additional metabolic support is compatible with the progressive length-dependent loss of axons observed in peripheral neuropathies (Spencer et al., 1978).

Although myelin was long thought to have a passive function in the nervous system, it is now well-recognized that the function and structural integrity of neurons depend on their continuous and reciprocal interaction with glial cells (Samara et al., 2013).

A growing body of evidence suggests that myelinating glial cells are able to provide trophic and metabolic support to axons to compensate for their physical insulation (Pellerin et al., 1998; Lee et al., 2012; Saab et al., 2013). To that end, the channel-like system of non-compacted myelin may serve as the path through which metabolites and trophic factors flow in direction to the adaxonal layer of myelin (Nave, 2010b). Notwithstanding with this potential functionality of the myelin structure, this function is presumably held by all axon-associated glial cells, since non-myelinating Schwann cells were shown to also protect the survival of sensory axons (Chen et al., 2003).

The first evidence for this glial function emerged from studies in the CNS, which gave rise to the astrocyte-neuron lactate shuttle hypothesis (ANLSH) (Pellerin et al., 1998). Blood-borne glucose represents the major energy substrate for the nervous system, being taken up by astrocytes in the CNS (Pellerin, 2003). Glucose is unlikely to be exported, since it is immediately phosphorylated by hexokinase, being instead used to produce pyruvate/lactate by glycolysis (Hirrlinger & Nave, 2014). Alternatively, astrocytes are enzymatically equipped to store it as glycogen, likely to be used under conditions of energy deprivation (Brown & Ransom, 2007; Chih et al., 2001). Lactate is then transferred to neurons and converted back to pyruvate, which undergoes oxidative metabolism in mitochondria to generate high amounts of ATP (Pellerin et al., 1998).

The ANLSH has been refined and the revised hypothesis includes the participation of oligodendrocytes in the shuttling of lactate in the CNS (Funfschilling et al., 2013; Lee et al., 2012;

Rinholm et al., 2011). Oligodendrocytes are able to import glucose either from the extracellular space or from astrocytes (with whom they are connected by connexins) to produce lactate (Rinholm & Bergensen, 2012). During myelination, they may consume it for energy production, as well as for lipid synthesis (Rinholm & Bergersen, 2014; Sánchez-Abarca et al., 2001). In mature CNS, glycolytic metabolism may yield sufficient energy to support oligodendrocyte survival and lactate is thought to be exported to the periaxonal space to metabolically support the underlying axon (Funfschilling et al., 2012; Lee et al., 2012; Rinholm & Bergersen, 2012).

Since the ANLSH emerged, a growing amount of studies have been done to explore the energy metabolism in the CNS, which is currently believed to be distributed across the three abovementioned cellular compartments (Amaral et al., 2013). Although less work has been devoted to PNS metabolism, emerging data also points to a division of metabolic activities between SCs and neurons (Brown et al., 2012; Chen et al., 2003; Viader et al., 2011). The exchange of energy substrates in the nervous system relies on the specific expression of connexins, glucose transporters (GLUT), monocarboxylate transporters (MCTs) and enzymes according to the metabolic tasks of the cells (Hirrlinger & Nave, 2014) (**Figure 4**).

Regarding the CNS, glucose enters the brain parenchyma via GLUT1 at the blood-brain barrier and is taken up by astrocytes through GLUT1, but also by oligodendrocytes and neurons through GLUT1 and GLUT3, respectively (Maher et al., 1994). Similarly in the PNS, GLUT1 is present in the perineurium and in the abaxonal side of Schwann cells, and GLUT3 mediates the uptake of glucose by the axon (Jensen et al., 2014).

Lactate shuttling requires particularly high lactate dehydrogenase (LDH) activity and rapid intercellular lactate transport (Hui et al., 2017). Lactate can only be used as a source of energy if oxidized to pyruvate via lactate dehydrogenase. Neurons express the LDH isoform LDH1, which preferentially uses lactate as substrate, whereas astrocytes express mostly LDH5, typically present in lactate-producing tissues (Bishop et al., 1972; Pellerin et al., 1998). The different distribution of these isoenzymes supports the idea that astrocytes might act as lactate sources for neurons to use it as energy substrate, in agreement with the ANLSH.

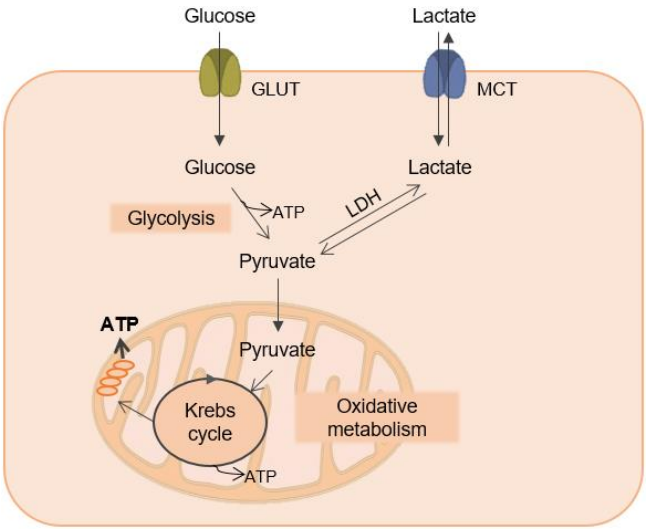

Figure 4. Graphic summary of reactions involved in cellular energy metabolism in the nervous system.

Lactate is exchanged between cells through MCTs. These transmembrane proteins perform also the proton-coupled transport of other monocarboxylates, namely pyruvate and ketone bodies, although at much lower extent (Halestrap, 2012). Four MCT types were functionally characterized, showing different affinities for monocarboxylates: MCT2 has a high affinity; MCT1 and MCT3 show an intermediate to high affinity, and MCT4 a low affinity (Bergersen et al., 2001; Grollman et al., 2000). Their selective presence in tissues tends to be related with their glycolytic versus oxidative phenotype. In the CNS, oligodendrocytes, neurons, and astrocytes predominantly express MCT1, MCT2, and MCT4, respectively (Lee et al., 2012). This cellular distribution of MCTs appear to be correlated with their main metabolic properties, which is consistent with the lactate shuttle hypothesis (Morrison et al., 2013).

Regarding the presence of MCTs in the PNS, our group has demonstrated the expression of MCT1, MCT2 and MCT4 by SCs, while MCT1 and MCT2 were found in mouse DRG neurons (Domènech-Estévez et al., 2015). A higher level of MCT1 expression was observed in maturing PNS, which suggested an increased need of monocarboxylates, presumably lactate, during that time (Domènech-Estévez et al., 2015). Regarding their spatial distribution, MCT1 was found in Schmidt-Lanterman incisures (SLIs) and in paradonal regions, both Cx32-rich structures composed by non-compacted myelin (Balice-Gordon et al., 1998; Domènech-Estévez et al., 2015). In turn, MCT4 was localized in the perinuclear and abaxonal compartments of mSCs, suggesting its presence in Cajal bands and in the outer cytoplasmic mesaxonal line (Domènech-Estévez et al., 2015). Altogether the available data indicate that each MCT isoform shows a preferred cellular distribution in CNS matching metabolic phenotype of glia and neurons (Domènech-Estévez et al., 2015). In the PNS, MCTs are expressed in different compartments of the SC-axon complex, potentially allowing lactate transport following a concentration gradient.

A schematic view of the main neuron-glia metabolic interactions in the CNS and PNS are shown in **Figure 5**.

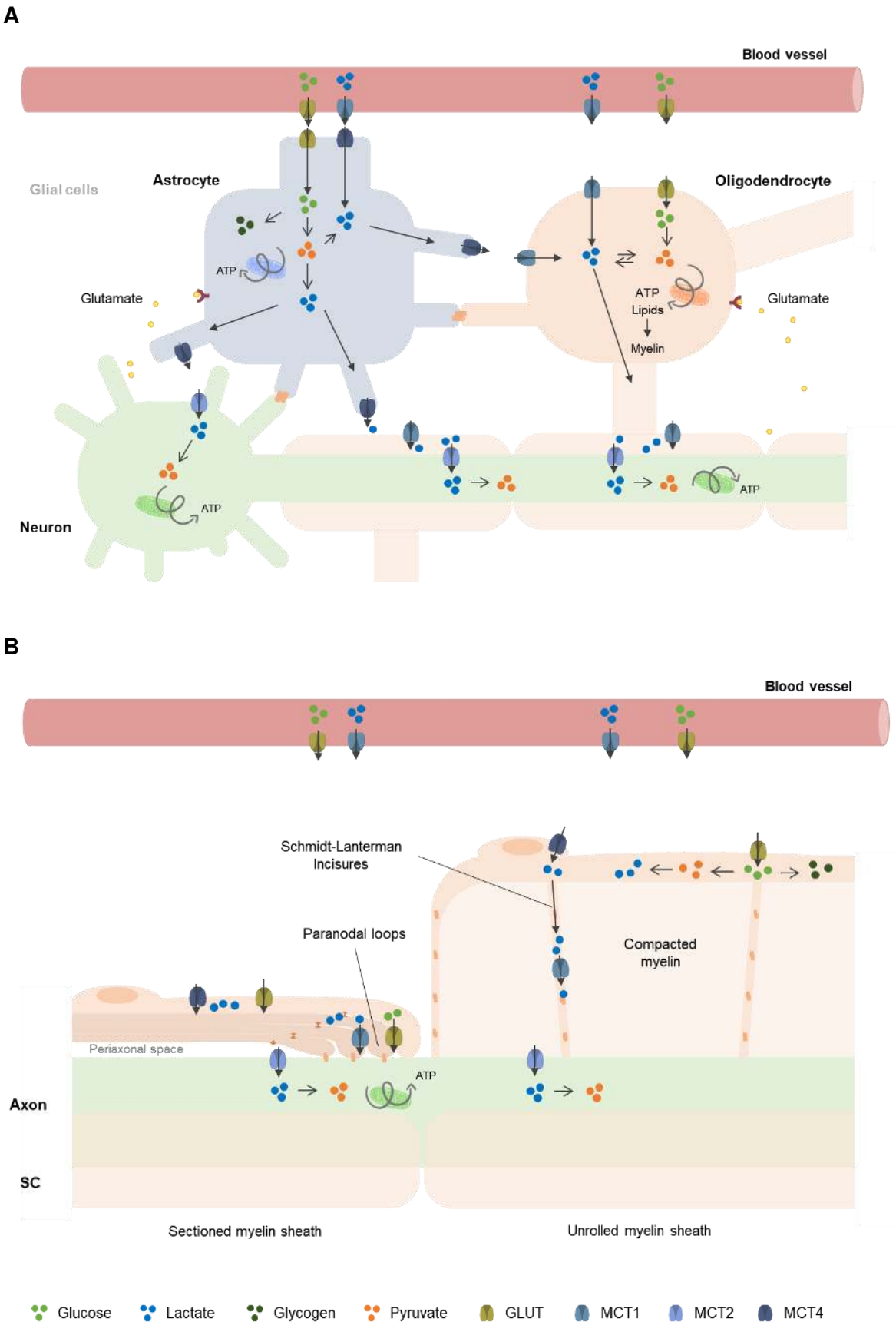

Figure 5. Schematic representation of the metabolic communication between neurons and glial cells in the CNS (**A**) and in the PNS (**B**).

1.3. Implications of disrupted SC-axon crosstalk

Several evidences for an axon-glia metabolic communication come from studies with animal models exhibiting axonal degeneration independently of myelin loss. Regarding the CNS, mice lacking oligodendroglia-specific genes *PLP1* (Garbern et al., 2002) and *CNP* (Lappe-Siefke et al., 2003) did not show extensive signs of impaired myelination but presented axonal degeneration. In the PNS, mouse mutants for the myelin-associated glycoprotein (MAG) presented axonal degeneration and decreased axon caliber in sciatic nerve fibers, despite their apparently normal myelination (Li et al., 1994). Moreover, SC-specific deletion of the metabolic regulator liver kinase B1 (LKB1) led to axon degeneration as a consequence of perturbed energy homeostasis independently of dysmyelination (Beirowski et al., 2014).

Given that lactate was proposed to be a crucial fuel for metabolic support to axons, it is not surprising that disrupting MCT1-mediated transfer of lactate from oligodendrocytes led to axonal damage (Lee et al., 2012). Importantly, in an *in vitro* experiment, the addition of free lactate to the medium rescued MCT1 blockage and ameliorated axonal phenotype, showing that neurodegeneration was due to decreased lactate export from oligodendrocytes and not import into neurons (Lee et al., 2012).

Similarly, axonal dysfunction in central and peripheral neuropathies may occur through myelin-unrelated mechanisms such as the failure of metabolic support.

Amyotrophic lateral sclerosis (ALS) is characterized by a progressive loss of motor neurons in the brain and spinal cord, also manifesting degeneration of peripheral fibers (Riva et al., 2014). Reduced levels of MCT1 expression in oligodendroglia were observed in superoxide dismutase 1 (SOD1)-mutant mice, a model of ALS and in brain samples from ALS patients (Lee et al., 2012). Together with the failure of mitochondrial bioenergetics (Ferri et al., 2006) and perturbations in axonal transport (Marinkovic et al., 2012), the lack of glial supply of lactate to motor neurons may also potentially be involved in the pathogenesis of ALS (Beirowski, 2013). Whether MCT dysfunction compromising SC-axon metabolic coupling is implicated in ALS pathogenesis is still unknown.

Peripheral neuropathies are a common cause of morbidity in elderly populations, representing a significant economic and societal burden (Hughes, 2002). The etiology for this type of peripheral neuropathies goes from metabolic irregularities (e.g. diabetic neuropathy) and genetic mutations (e.g. Charcot-Marie-Tooth diseases) to inflammation (e.g. demyelinating polyneuropathies) and infection (e.g. leprosy) (Samara et al., 2013).

Heritable peripheral neuropathies are collectively designated as Charcot-Marie-Tooth diseases (CMT). Most of the genes mutated in CMT play a role in maintaining the structure or function of the axon-SCs complex formed by and motor/sensory neurons (Saporta & Shy, 2014). CMT neuropathies cause distal muscle weakness and atrophy, and they can be roughly divided into demyelinating (CMT1), axonal (such as CMT2) and more rare intermediate variants (Timmerman et al., 2013). As in some forms of CMT2 disease the neurodegeneration occurs in the absence of detectable changes in myelin integrity, the disruption of metabolic support of the

peripheral neurons may also be implicated in the pathogenesis of this CMT variant (Timmerman et al., 2013). This hypothesis is further supported by the observation that many types of peripheral neuropathies exhibit deficits in axonal energy, such as mitochondrial dysfunction, as a common feature (Beirowski et al., 2014; Viader et al., 2011).

In order to develop new therapeutic approaches to treat or at least improve the quality of life of people suffering from these diseases, it is crucial to explore the metabolic SC-axon communication in physiological and pathological conditions.

1.4. Aim, Hypothesis and Strategy

Both neurons and glia play critical roles on nervous system homeostasis, and abnormalities in their relationship are at the core of innumerous neuropathic disorders. The delivery of high-energy substrates from glial cells to neurons via MCTs may be one of the most important events underlying their communication. Although much work has been done to explore CNS metabolism, comprehensive knowledge regarding the physiological relevance of glia-axon metabolic support and the role of MCTs in the PNS is still missing.

Therefore, the aim of this master's thesis is:

1. To explore SCs' metabolic adaptations to neuronal cues, in particular lactate flow and production;
2. To study the role of monocarboxylate transporters in SCs *in vivo*.

Firstly, we hypothesized that extrasynaptically released neurotransmitters interact with receptors in SCs, triggering the activation of certain signaling pathways associated with the reprogramming of their metabolic status. We believe that it would enhance lactate uptake and/or glycolytic metabolism leading to increased intracellular levels of lactate. This monocarboxylate would then be shipped to the periaxonal space and taken up by the axon through MCTs, finally undergoing oxidative metabolism to provide the energy needed for signal transmission along the axon.

To test these hypotheses, we elaborated a strategy divided into *in vitro* studies and *in vivo* approaches. First, we intended to evaluate whether signaling pathways reported to precede metabolic shifts are activated in cultured SCs in response to glutamate. To do that, we compared the phosphorylation levels of proteins involved in these pathways between stimulated and non-stimulated cultures using Western Blot. Additionally, we planned to monitor the intracellular levels of lactate in SCs upon glutamate exposure, by performing continuous FRET imaging of cultured SCs expressing a lactate-sensitive probe. Lastly, we aimed to characterize conditional knock-out mouse models where MCT1 or MCT4 were specifically deleted in SCs to study their physiological role *in vivo* and their importance for axon-SC metabolic communication. The validation of the mouse models and the effects of MCT depletion were assessed by immunohistochemistry and quantitative PCR, among others.

A schematic summary of our hypotheses and strategy is shown in **Figure 6**.

Hypothesis

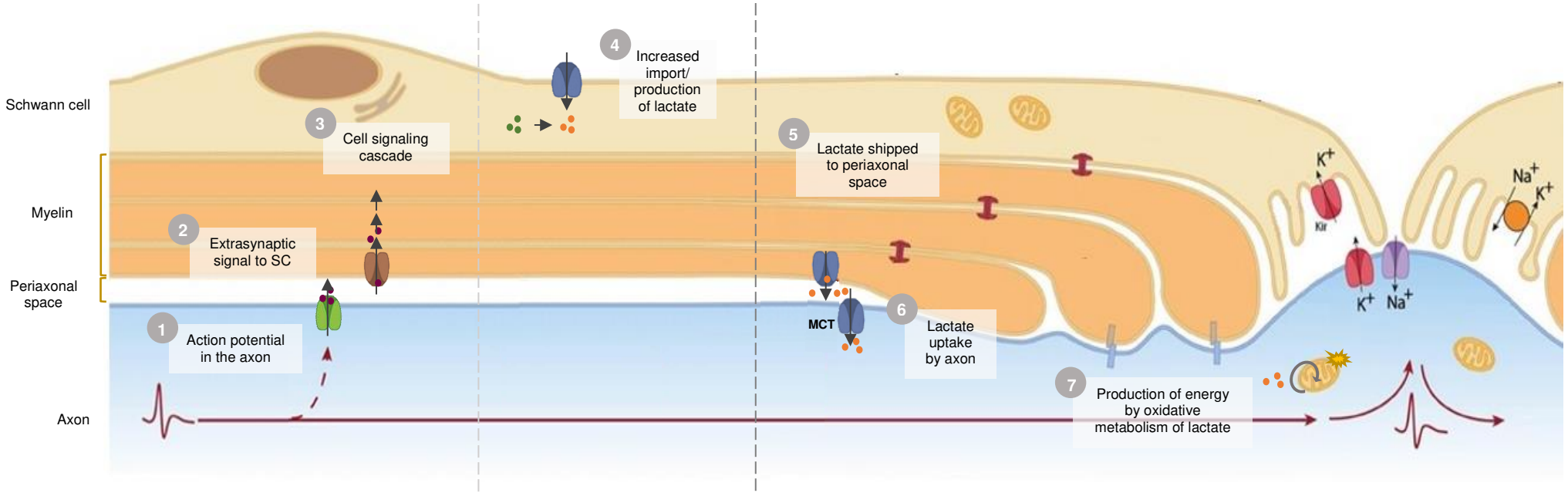

Strategy

A Evaluate whether signaling pathways related with metabolic shifts are activated in cultured SCs upon glutamate exposure

B Monitor intracellular levels of lactate in cultured SCs upon glutamate exposure

C Characterize conditional knock-out mouse models where MCT1 or MCT4 were specifically deleted in SCs to study their physiological role *in vivo* and their importance for axon-SC communication

In vitro studies | *In vivo* studies

Western Blotting | FRET | q-PCR, Immunohistochemistry, among others

Figure 6 - Hypothesis and Strategy. Adapted from (Samara et al. 2013)

2. Materials and Methods

2.1. Reagents

Buffers and Solutions

Lysis buffer (for protein): 80mM TrisHCl (Duchefa Biochemie, T1513.1000); 5 mM EDTA (Sigma-Aldrich, 101520387), 5% SDS (Sigma-Aldrich, 101944022), 1 mM NaF (Sigma-Aldrich, S7920), 1 mM $NaVO_4$ (AppliChem, A2196.0005) and protease inhibitor cocktail 1X (complete Mini-EDTA-free tablets; Roche, 11836170001)

Running buffer: 25 mM Tris base (Sigma, 101776239, USA), 192 mM glycine (AppliChem, A4554.5000) and 0.1% SDS (AppliChem, A3942.1000) in distilled water

Transfer buffer: 25 mM Tris base (Sigma, 101776239), 192 mM glycine (AppliChem, A4554.5000), and 20% methanol (Honeywell, 24229-2.5L-R) in distilled water

Tris-buffered saline (TBS): 20 mM Tris base (Sigma, 101776239) and 150 mM NaCl (Honeywell, 10314835) in distilled water, pH 7.5

Blocking buffer (for WB): 5% non-fat dried milk (AppliChem, A0803.1000) in TBS

TBS Tween: 0.05% Polysorbate 20 (Duchefa Biochemie, P1362.1000) in TBS

Phosphate buffer saline (PBS): 137mM NaCl (Honeywell, 10314835), 2.7mM KCl (VWR, 26764.260), 10mM Na_2PO_4 (Sigma, S-0751), 1.7mM KH_2PO_4 (VWR, 26764.260), pH7.5

Krebs-Ringer-HEPES (KRH) buffer: 112mM NaCl (Honeywell, 10314835), 1.25mM $CaCl_2$ (Sigma-Aldrich, 10314835), 1.25mM $MgSO_4$ (Sigma-Aldrich, 101928373), 10mM HEPES (AppliChem, A3724.0100), 24mM $NaHCO_3$ (Merck, 1.06329.0500), 5mM KCl (VWR, 26764.260) in distilled water

Lysis Buffer (for DNA): 0.5 mg/mL Proteinase K (Merck, 1.24568) added to 100mM NaCl (Honeywell, 10314835), 50mM Tris-HCl pH8.0, 100mM EDTA (Sigma-Aldrich, 101520387), and 1% SDS (Sigma-Aldrich, 101944022)

Phosphate buffer (PB) 0.1M: $Na_2PO_4.2H_2O$ (Honeywell, 10314743), 0.1M NaH_2PO_4 anhydrous (Sigma-Aldrich, RDD007) in distilled water, pH7.2

Zamboni fixative: 2% paraformaldehyde (PFA; AppliChem, A3813.0500) with 15% Picric Acid (Sigma-Aldrich, 239801) in PB, pH7.3

Cell culture

Poly-L-Lysine (PLL) coating: 0.1 mg/ml PLL (Sigma, P1274) in PBS

SC culture medium: DMEM 1X + GlutaMAX (Gibco, 61965-026) supplemented with 10% fetal bovine serum (FBS; Gibco, 16000-044), 50 U/ml penicillin, 50 µg/ml streptomycin (Gibco, 15070063), 4 µM forskolin (LC labs, 66575-29-9), and 1.25 nM EGF domain NRG1b1 (R&D Systems, 396-HB). DMEM contains 0.4 mM glycine.

Bovine pituitary extract (Lonza Biosciences, CC-4009) (working solution: 21mg/mL)

Glutamate: L-Glutamic acid monosodium salt hydrate (Sigma-Aldrich, 1002218638)

HEK293T culture medium: DMEM 1X + GlutaMAX (Gibco, 61965-026), 10% FBS (Gibco, 16000-044), 50 U/ml penicillin, 50 µg/ml streptomycin (Gibco, 15070063), 1X Non-Essential Amino Acids solution (Gibco, 11140050) and 1 mM Sodium Pyruvate (Gibco, 11360).

2.2. Glutamate stimulation of primary cultured SCs

Cell culture

Rat Schwann cells were obtained from sciatic nerves, extracted from 1-3 days old Sprague Dawley rats, and prepared as previously described (Brockes et al., 1979).

Cells were plated in PLL-coated 6 cm Petri dishes, at a starting density of 4 million cells/dish, maintained in SC culture medium and passaged no more than 6 times.

Immunoblot analysis of cell signaling

Cultures were rinsed twice in PBS and exposed to starving and stimulation media as described in detail in the 'Results and Discussion' section.

After stimulation, cells were rinsed twice in PBS, lysed with 150 µL lysis buffer, and scraped with a plastic spatula. Lysates were collected, further homogenized in the Tissue Lyser II (Qiagen) with steel beads and centrifuged 20 min at 13000g in Centrifuge 5415D (Eppendorf).

Protein concentration was estimated for each cell lysate by PierceTM bicinchoninic acid assay (BCA; Thermo Scientific, 23225) and absorbance was determined at 562 nm using PlateReader (Biotek).

Equivalent amounts of protein were loaded into a 10% SDS-PAGE gel, along with molecular weight marker (Precision Plus Protein Standards; BIO-RAD, 161-0373). Proteins were electrotransferred to nitrocellulose membranes. Membranes were blocked for 1h with blocking buffer, incubated overnight at 4ºC with primary antibodies, and with secondary antibodies for at least 1h20 at room temperature (RT) (**Table 1**). Immunoblots were analyzed using the LI-COR Odissey system (Biosciences) as recommended by the company. The results were expressed as the ratio of phopsphrylated/total protein, following the normalization to tubulin.

Table 1. List of primary and secondary antibodies used for Western Blot.

Primary antibodies				
Antigen	Animal of origin	Dilution	Product reference	
P-AKT (S473)	Rabbit	1:1000	Cell Signaling, 3787	
P-ERK (T202/Y204)	Rabbit	1:1000	Cell Signaling, 9101	
P-S6RP (S235/236)	Rabbit	1:1000	Cell Signaling, 2211	
AKT	Rabbit	1:1000	Cell Signaling, 9272	
ERK	Rabbit	1:1000	Cell Signaling, 9102	
S6RP	Rabbit	1:1000	Cell Signaling, 2217	
Tubulin	Mouse	1:5000	Cell Signaling, 3873	
Secundary antibodies				
Antigen	Conjugated fluorophore	Animal of origin	Dilution	Product reference
Rabbit IgG	IRDye® 800CW	Goat	1:10000	LI-COR 925-32211
Mouse IgG	IRDye® 680RD	Donkey	1:10000	LI-COR 925-68072

2.3. FRET-based intracellular lactate measurements

Approximately 40 000 HEK 293T cells (Thermo-Fisher Scientific) were plated onto PLL-coated 18 mm coverslips, and transfected 48h later with LipoD293 (SignaGen) and 0.75mg of Laconic DNA, according to the indication of the manufacturer (San Martín et al., 2013).

24h after transfection, cells were imaged at the Advanced Light Microscopy Facility (Science for Life Laboratory, Stockholm, Sweden) using a 10x air objective, in the absence of atmospheric control.

Cells were exposed to different solutions prepared in KRH buffer, as detailed in 'Results and Discussion' section, at a perfusion temperature of 37ºC. Laconic behavior at each condition was monitored during 5 minutes, and data was finally presented as mTFP/Venus fluorescence ratio in function of the time, normalized to the first fluorescence ratio acquired at steady-state.

2.4. Characterization of the mouse models

Animals

Conditional knockout (cKO) mice expressing Cre recombinase under the promoter for P0 and floxed MCT1 or MCT4 alleles were provided by our collaborator Dr. Luc Pellerin's group at the University of Lausanne, Switzerland. The P0-Cre line is commercially available from Jackson Labs (B6N.FVB-Tg(Mpz-cre)26Mes/J) (M. A. Feltri et al., 1999). The floxed lines were developed by Cyagen (Switzerland).

Ablation of MCT1 expression is driven by the excision of exon 5 of gene *SLC16A1*. In turn, deletion of MCT4 expression occurs through the elimination of exons 3, 4 and 5 of *SLC16A3*.

All experiments were performed in accordance with the guidelines of Karolinska Institute.

Genotyping

DNA from mouse ear or tail clips was extracted by incubating samples at least 4 hours at 56ºC with lysis buffer, and by alternating centrifugations with the sequential addition of 5M NaCl, isopropanol and ethanol 70%, and finally resuspended in TE buffer.

A cocktail of PCR reagents was prepared by mixing primers (0.2µM at working solution; **Table 2**) with DreamTaq Master Mix (ThermoFisher, K1082) in nuclease-free water. The cocktail was added to 0.5µL DNA, undergoing a PCR reaction (**Table 3**).

PCR products were resolved in a 1-2% agarose gel by electrophoresis (Agarose, Fisher Scientif, BP160-500; GelRed Nucleic Acid Stain, 41003; Ready-to-use 100bp DNA ladder, 31032, Biotium). The gel was visualized using ChemiDoc (BIO-RAD).

Table 2. Primer sequences used for genotyping PCR.

Gene	Primer Forward	Primer Reverse
MCT1	5'-AGACTTGGGTAACTGAATGATGCTGACT-3'	5'-TCCAAGGACAGCCAAGCTACATAGAG-3'
MCT4	5'-ATTTAGACTCAGAGGTGGGCAGAGTG-3'	5'-TTGCCAGGGTGACCATCTCA-3'
P0-Cre	5'-AGGTGTAGAGAAGGCACTTAGC-3'	5'-CTAATCGCCATCTTCCAGCAGG-3'
IL-2	5'-CTAGGCCACAGAATTGAAAGATCT-3'	5'- GTAGGTGGAAATTCTAGCATCATCC-3'

Table 3. Programs used for PCR Reaction.

	Floxed MCT1/ MCT4			P0-Cre		
	Temperature	Time	Cycles	Temperature	Time	Cycles
Initial denaturation	94 ºC	3 min	1	94 ºC	3 min	1
Denaturation	94 ºC	30 s	35	94 ºC	15 s	32
Hybridization	55 ºC	30 s		62 ºC	15 s	
Extension	72 ºC	30 s		72 ºC	15 s	
Final extension	72 ºC	10 min	1	72 ºC	2 min	1
Conservation	4 ºC	pause	-	4 ºC	pause	-

Quantitative Real-Time Polymerase Chain Reaction (RT-qPCR)

RNA from the endoneurium of mouse sciatic nerves was extracted using RNeasy Lipid Tissue Kit (Qiagen 74804), following the manufacturer's instructions. Briefly, tissue was homogenized in 500µL QIAzol (QIAGEN, 79306) and RNA fraction was extracted using

chloroform (Sigma-Aldrich, 101538376). RNA was then purified in column using the reagents provided in the kit. Residual contaminating DNA was digested with RNAse free DNAse set (QIAGEN, 79254). Next, RNA concentration was determined using NanoDrop 1000 (Agilent). Finally, 40ng RNA was retrotranscribed with PrimeScript RT reagent Kit (Takara RR037A), according to the manufacturer's recommendations (**Table 4**).

MCTs, P0 and Ubiquitin-conjugating enzyme E2 L3 (Ubiq) mRNA levels were detected by quantitative real-time PCR using FastStart Universal SYBR Green Master Mix (Roche, 10356100) and 7500 Fast Real Time PCR System (Applied Biosystems).

Oligonucleotides sequences used are shown in **Table 5** and qPCR protocol in **Table 6**.

Table 4. Retrotranscription protocol.

	Temperature	Time
Reverse transcription	37 ºC	15 min
Inactivation of reverse transcriptase	85 ºC	5 s
Conservation	4 ºC	pause

Table 5. Primer sequences used for qPCR.

Gene	Primer Forward	Primer Reverse
MCT1	5'-AATGCTGCCCTGTCCTCCTA-3'	5'-CCCAGTACGTGTATTTGTAGTCTCCAT-3'
MCT2	5'-CAGCAACAGCGTGATAGAGCT-3'	5'-TGGTTGCAGGTTGAATGCTAA-3'
MCT4	5'-CAGCTTTGCCATGTTCTTCA-3'	5'-AGCCATGAGCACCTCAAACT-3'
P0	5'-AGCCCCAGCCCTATCCTGGC-3'	5'- GCAGTGCAGGGTCACCTGGG-3'
Ubiq	5'-CAGCCACCAAGACTGACCAA-3'	5'-CATTCACCAGTGCTATGAGGGA-3'

Table 6. qPCR protocol.

	Temperature	Time	Cycles
Activation	50 ºC	2 min	1
Denaturation	95 ºC	10 min	1
Denaturation	95 ºC	15 s	40
Extension	60 ºC	1 min	
Melting curve	95 ºC	15 s	1
	60 ºC	1 min	1
	95 ºC	15 s	1

Immunohistochemistry

Adult animals were anesthetized intraperitoneally with a mixture of 10 µL/g of Ketanarkon 100 (1 mg/ml, Streuli) with 0.1% Rompun (Bayer) in PBS, sacrificed by cervical dislocation, and dissected to collect sciatic nerves, muscles (gastrocnemius, tibialis, soleus, extensor digitalis longus (EDL)) and hind paw skin. Tail was also collected for validation of the previously performed genotyping.

After fixations, tissues were cryoprotected (sucrose 20% overnight at 4ºC), embedded in optimal cutting temperature medium (OCT; Cell Path, KMA-0100-00A), and sectioned according to **Table 7**.

Tissues were immunostained following the procedures detailed below. Images were then acquired using Zeiss LSM 700 confocal microscope and processed with FIJI software (Schindelin et al., 2019).

Table 7. Settings for fixation and sectioning of different tissues.

Tissue	Fixation	Sections	Thickness
Sciatic nerve	4% PFA; 1h	Transversal	10 µm
Gastrocnemius	4% PFA; 15 min	Longitudinal	25 µm
Tibialis			
Soleus	4% PFA; 10 min		
EDL			
Hind paw skin	Zamboni fixative; 2h	Transversal	50 µm

Teased fibers of sciatic nerve

PFA-fixed fixed mouse sciatic nerves were stripped of perineurium and small bundles of fibers separated using thin needles. Individual myelinated fibers were spread on a TESPA (Sigma-Aldrich, 101698432)-coated glass slide, allowed to dry and stored at -80ºC until used.

For immunostaining, samples were initially washed with PBS and permeabilized with 0.2% Triton X-100 for 15 min at RT. Afterwards, fibers were blocked with 1% BSA and 0.2% Triton X-100 for 1h at RT, and incubated with primary antibodies overnight at 4ºC or RT (**Table 8**). Next, samples were washed and fluorescently labeled with secondary antibodies for 2h at RT (**Table 8**). Lastly, nuclei were counterstained with DAPI and tissues were mounted with Vectashield.

Cross sections of sciatic nerve

10µm-thick cryosections of mouse sciatic nerve were washed with PBS and permeabilized as previously described. Secondly, samples were blocked and incubated with primary antibodies overnight at 4ºC or RT (**Table 8**). Next, sections were washed, incubated with secondary antibodies and counterstained with DAPI (**Table 8**) before mounting with Vectashield.

Intraepidermal nerve fibers

Hind paw skin was sectioned at 50 µm thickness, blocked with 1% NGS and 0.15% Triton X-100 for 3h at RT and incubated with primary antibodies overnight at 4ºC. Next, sections were fluorescently labeled with secondary antibodies for 2H at RT, stained with DAPI and mounted.

Z-stacks were obtained from four different frames of three or more sections per animal. The number of intraepidermal fibers was counted and normalized to the length of dermal-epidermal junction in the superimposed image.

Neuromuscular junctions

Muscle sections were washed with PBS, and blocked with 4% BSA and 0.5% Triton X-100 for 5h at RT. Then, samples were incubated with primary antibodies (**Table 8**) for 48h at 4ºC, washed and stained with secondary antibodies (**Table 8**) for 2h at RT. Finally, samples were counterstained with DAPI and mounted.

Table 8. List of primary antibodies, secondary antibodies and stains used for immunohistochemistry.

Primary antibodies				
Antigen	Animal of origin	Dilution	Product reference	
MCT1	Rabbit	1:200	Homemade	
MCT4	Rabbit	1:200	Santa Cruz sc-50329	
Neurofilament-145	Rabbit	1:200	Millipore AB1987	
Neurofilament-200	Mouse	1:400	Sigma N0142 Clone N52	
PGP9.5	Rabbit	1:400	Ultraclone RA95101	
Secundary antibodies				
Antigen	Conjugated fluorophore	Animal of origin	Dilution	Product reference
Mouse IgG	Alexa Fluor® 488	Goat	1:200	Life Tech R37120
Mouse IgG	Alexa Fluor® 594	Goat	1:200	Life Tech R37121
Rabbit IgG	Alexa Fluor® 488	Goat	1:200	Life Tech A11034
Rabbit IgG	Alexa Fluor® 594	Goat	1:200	Life Tech A11037
Stains				
	Conjugated fluorophore	Dilution	Product reference	
α-Bungarotoxin	Alexa Fluor® 488	1:500	Thermo Scientific B13422	
Phalloidin	Alexa Fluor® 488	1:20	Thermo Scientific A12379	
4',6-Diamidino-2-Phenylindole, Dihydrochloride (DAPI)		1:10000	Sigma-Aldrich D9542	

3. Results and Discussion

3.1. *In vitro* study of the intracellular response of SCs to neurotransmitters

Active axons can release ATP and glutamate (Glu) into the narrow periaxonal space, where they reach high local concentrations (Samara et al., 2013; Stys, 2011). Myelinating and non-myelinating SCs, as well as their common precursors, express various ion channels and G protein-coupled receptors at their surface that may act as activity sensors. Purinergic and glutamatergic receptors are among this set of proteins, so that SCs can detect ATP and Glu as extrasynaptic signals of axonal activity (Samara et al., 2013).

In the CNS, it was suggested that neuronal activity induces astrocytes and oligodendendrocytes to provide metabolic substrates and enzymes to neurons (Barros, 2013; Frühbeis et al., 2013). Peripheral glia may play a similar role by providing the metabolic support to axons.

In order to dissect whether (and how) the metabolic status of SCs is modulated by neuronal activity, we devised a strategy to assess the amplitude of lactate production and release by cultured SCs when stimulated by glutamate. If SCs promptly increase the generation of glycolysis products to support axons during periods of their activity, short-term exposure of SCs to neurotransmitters should be enough to trigger a feedback response.

With this in mind, we first evaluated whether rat SCs in our cell-culture settings were able to readily sense the presence of glutamate and initiate a feedback response through the activation of metabolism-related signaling pathways. Once we confirm that SCs in our *in vitro* system are responsive to glutamate and we establish a reliable protocol of glutamate-driven SC stimulation, we can use it coupled with a FRET system to screen potential fluctuations of the SC's intracellular level of lactate arising from glutamate signaling. Hence, we worked in parallel on setting up a FRET imaging system for cultured cells expressing Laconic, a lactate-sensitive FRET probe (San Martín et al., 2013). As an initial attempt to reproduce the method using the available protocol for Laconic, we exposed HEK293T cells expressing Laconic to solutions that were reported to cause specific signal emission.

Of note, this *in vitro* approach is still ongoing and no conclusive data will be presented. A long series of optimization steps were needed to be carried out for the establishment of both systems.

3.1.1. Cell signaling cascades triggered in cultured SCs by glutamate exposure

During neuronal activity, glutamate extrasynaptically secreted by axons can interact with either ionotropic or metabotropic receptors in SCs (Verkhratsky & Kirchhoff, 2007). The former are ligand-gated ion channels subdivided into NMDA, AMPA and kainate receptors, which exhibit distinct functional properties (Verkhratsky & Kirchhoff, 2007). Metabotropic glutamate receptors (mGluR), in turn, are G-protein-coupled receptors that control intracellular second messenger signaling cascades. In comparison with ionotropic receptors, mGluR tend to be activated by a

stronger and/or longer stimulus (Verkhratsky & Kirchhoff, 2007). As such, following the abovementioned strategy to test if SCs promptly respond to axonal cues of activity, we expect to trigger ionotropic signaling in SCs shortly exposed to low concentrations of glutamate.

Recently, it was reported that ionotropic glutamate stimulation in primary rat SC cultures triggered the robust activation of PI3K/AKT/S6RP and ERK signaling pathways, in particular through interaction with NMDA receptors (Campana et al., 2017). These signaling pathways may be associated with glycolytic metabolism (Bhaskar & Hay, 2007; Marat & Haucke, 2016; Perkinton et al., 2002). The response was transient and bimodal, peaking upon a treatment of 80 µM glutamate for 20min and ceasing when glutamate concentrations exceeded 250 µM. This work matched perfectly the first part of our hypothesis. Thus, we followed the same protocol (Campana et al., 2017) as an attempt to replicate the outcome in our cell cultures, since more or less defined parameters in *in vitro* contexts can influence the type or magnitude of the effect.

The methodology involved starving subconfluent rat SCs for 1 hour in serum-free medium in order to reduce their metabolism to the basal levels. Then, different concentrations of Glu were applied for 10min, the proteins were extracted from treated and non-treated cells, and the levels of total and phosphoryled AKT, S6RP and ERK were assessed by Western Blot (WB) (**Table 9**, step 1). Surprisingly, in our cell culture settings, no apparent effect of Glu was observed. The removal of fetal bovine serum (FBS), even when combined with the absence of pituitary extract, was not sufficient to reduce the cell metabolism to the baseline, which is required to reveal the specific response to Glu. Exploring the small deviations from the reported protocol, we found that loading half of the protein mass into the WB gel could be a potential cause for such outcome.

Moreover, whereas enhanced chemiluminescence (ECL) was the method adopted by Campana and colleagues for WB detection, we used Odyssey® Infrared Imaging System. We believe that this divergence is not a limiting factor. On the contrary, infrared imaging counteracts the dynamic light-producing enzymatic reactions on which ECL relies, suppressing this way the need for optimizing reaction times and imaging (Mathews et al., 2009). Furthermore, the highly-sensitive method that we used allows a broader detection range than ECL and the simultaneous imaging of different proteins on the same blot, which increases the detection efficiency.

In order to enhance the outcome of Glu-mediated stimulation of SCs, we used a multi-step optimization process (**Table 9**). We changed the culture medium to contain Nrg1 type III instead of bovine pituitary extract (BPE), as the latter possess undefined – and possibly variable – composition. We also performed the next assay on confluent populations of SCs as a way to collect more proteins from each culture plate (**Table 9**, step 2). Since we obtained a good outcome from the first optimized stimulation of confluent cells, we presumed that high cell density allowing us to have enough material would not be a parameter negatively affecting the outcome of our experiments. Additionally, we tried to strengthen SC starving step to lower their metabolic baseline (**Table 9**, steps 3-4).

In parallel, as a way to prevent operation errors, we minimized the number of conditions to test, doing also technical replicates for each condition. Since we were interested on evaluating the shortest axonal stimulation that triggers a glial response, we tested exposing cells for 5 min

to 40 µM or 80 µM glutamate, concentrations described to induce the stronger effect, in comparison with 20 min-long stimulation.

The initial trials of cell starvation exhibited variable efficiency, even when the experiment was repeated using the same settings. An activation of AKT and/or ERK pathways following Glu exposure was visible when the starving was successful. A rise in ERK phosphorylation was observed specially for 5 min-long treatment with Glu. However, the results regarding the AKT signaling pathway were not linear. The phosphorylation of AKT was either robust or absent, while no clear effects on S6RP phosphorylation were observed.

We found in the literature that Glu at high concentration (2 mM) signals through metabotropic glutamate receptors in SCs to enhance Nrg1-induced phosphorylation of ERK, but not AKT (Saitoh et al., 2016). In that work, the metabolic baseline of primary cultured SCs was reached after starving cells during 6h in 1% FBS medium, and Glu stimulation was done for 30min in the presence of different picomolar concentrations of Nrg1 type III. Bearing this in mind, we questioned whether ionotropic glutamate signaling in SCs may similarly modulate ErbB receptor-mediated cellular signaling.

To test this possibility, we tried to combine the approaches described in the two referred papers (**Table 9**, steps 5-6). After the application of an optimized starving method, subconfluent cultured SCs were stimulated for 10 min with Nrg1 at concentrations ranging from tens of picomolar to few nanomolar, in the absence or presence of 80 µM glutamate. Cells efficiently reached the basal levels of activity, and usually the magnitude of activation of AKT/S6RP and ERK signaling increased in function of the concentration of Nrg1. Intriguingly, the addition of Glu generally decreased the effect induced by Nrg1, with exception of one assay where AKT phosphorylation was enhanced by Glu in the presence of at least 0.1 nM Nrg1. Furthermore, Glu alone induced variable types of response, either reducing or increasing the phosphorylation of the ERK, AKT and/or S6RP.

We supposed that the level of cell confluence may have largely influenced the outcome. Cultured SCs displayed ~85% confluence at the onset of the experiments as suggested by Campana and colleagues (2017). However, the method of starving described in the same article was substantially weaker compared to the treatment that we adopted. We observed that in standard culture conditions, our rat SCs would continue to replicate until the cytoplasm was compacted and little space would be visible between cells. Consequently, subconfluent cells may rely more on the presence of nutrients and growth factors, and may be more susceptible to starving-induced stress. As such, SCs in this set of tests may be more stressed upon starvation induced by removal of Fsk and Nrg1 from the culture medium for 24h plus FBS for 2h. The fact that AKT/S6RP signaling is also associated with survival responses and that stress activates ERK signaling (Yarden & Sliwkowski, 2001) can potentially explain the observed phenotype. We believe that exposing subconfluent SCs to a strong starvation regime induces more stress. In this context, residual levels of Nrg1 may trigger the activation of AKT/S6RP and ERK signaling in order to generate the survival response to stress. The additional presence of Glu seems to counteract the survival response of SCs to Nrg1. In line with our hypothesis, glutamate may signal

the metabolic demands of axons to SCs, leading to the glial mobilization of energy reserves, which are already depleted under these conditions. Thus, we believe that cell confluence is a critical factor to take into account in these experiments.

Having this in mind, we lastly followed the same procedure on a confluent culture of rat SCs, adding Nrg1 at concentrations in the order of hundreds of picomolar, alone or combined with 80 µM glutamate (**Figure 7**). Under these conditions, the presence of Glu appeared to enhance the Nrg1-induced phosphorylation of AKT, S6RP, and ERK. Moreover, the effect of Glu was visible even in the absence of Nrg1, and peaked when the lowest concentration of Nrg1 was added to the culture (**Figure 8**).

Firstly, these observations suggest that cell confluence is an important parameter to take into consideration in our experimental settings. Indeed, when cells in culture are establishing more and tighter contacts with each other, they form a more stable cell population. That means that confluent cells are less sensitive and can adapt much more efficiently to stress conditions. We further suppose that it can result in more consistent responses to external factors. Nevertheless, this experiment has to be repeated exactly with the same technical conditions to evaluate the reproducibility of the outcome.

Additionally, it seems that the number of times that SCs are passaged in culture influences the type of response triggered by stimulation. In Campana et al. (2017), it was mentioned that cells used were passaged no more than 7 times. We followed this indication without attention if a given protocol was repeated on cells at the same passage level. However, it may have compromised the replication of the results. Having a look on the assays number 2 and 3 where only Glu stimulation was tested (**Table 9**), there are clear differences on the type of response exhibited by confluent cells at the fourth passage (P4) versus at the sixth passage (P6) exposed to the same experimental settings. The metabolic baseline, as well as a robust Glu-induced increase of Erk and/or Akt phosphorylation, were reached in both tests for cells at P6; whereas a mild efficacy of the starving and a low phosphorylation of AKT and ERK were observed in cells at P4 in the best case scenario.

This difference may partially follow differences in physiological events in the developing versus mature PNS. In fact, since myelin-forming cells are highly energy demanding during lineage progression and particularly myelination (Rinholm et al., 2011; Sánchez-Abarca et al., 2001), it is plausible to assume that glia-to-axon metabolic support does not occur or is minimized at that period. In mature PNS, in turn, a growing body of evidence supports the idea that SCs provide axons with metabolites, as we intend to prove during neuronal activity. Thus, even though we used confluent cultured cells, the state of cell maturity (as reflected by the number of SC passages) may modulate their plasticity to develop physiological adjustments through subcellular signaling upon stimulation with neurotransmitters.

Table 9. Main steps of optimization for the glutamate stimulation of cultured rSCs and respective outcomes (continues on the next page).

	Purpose	Culture	Starving	Stimulation	Observations	*n*
1	Follow procedure described in *Campana et al.* (2017)	~85% cell confluence SCs at passage no. 4 FBS/Fsk/BPE in DMEM	Fsk/BPE in DMEM; 1h	0, 20, 40, 80, 100, 250, 500, 2000 µM Glu Positive Ctr: Nrg1 5nM 10 min	Low mass of protein loaded Baseline not reached Total AKT, ERK and S6RP variable	1
			Fsk in DMEM; 1h		No reproduction of phosphorylation levels	1
2	Load 40µg protein Use media with more defined composition Reduce number of conditions-test	~98% cell confluence a) SCs at passage no. 6 b) SCs at passage no. 4 FBS/Fsk/Nrg1 in DMEM	Fsk/Nrg1 in DMEM; 1h	0, 40, 80 µM Glu 5, 20 min a) No replicates b) 3/4 replicates	a) Baseline reached Robust phosphorylation of AKT and ERK (the longer/stronger exposure the less robust) b) Baseline not reached Low phosphorylation of AKT and ERK (peaking at 5min 80µM Glu)	2
3	Test a longer and stronger starving	~98% cell confluence a) SCs at passage no. 6 b) SCs at passage no. 4 FBS/Fsk/Nrg1 in DMEM	Fsk in DMEM; 5-6h	0, 40, 80 µM Glu 5, 20 min Triplicates	a) Baseline reached Robust phosphorylation of ERK, particularly for 5min Glu exposure AKT/S6RP signaling pathway seems to be unaffected by Glu exposure b) Less efficient starving Total AKT, ERK and S6RP variable Robust phosphorylation of ERK only for 5min Glu exposure Low phosphorylation of S6RP but not AKT	2
4	Test an even longer and stronger starving	~98% cell confluence SCs at passage no. 4 FBS/Fsk/Nrg1 in DMEM	Fsk in DMEM, 5-6h FBS in DMEM, 24h + DMEM 2h	0, 80 µM Glu Positive Ctr: Nrg1 5nM 5 min Duplicates	The longer starving is even more efficient, and cells are still responsive to stimuli Signal coming from the stimulated cells is weaker in the longer starving	1

5	Test whether Glu enhances the effect of Nrg1 at concentrations tested in *Saitoh et al*. (2016) on a subconfluent culture as used in *Campana et al.* (2017)	~85% cell confluence a) SCs at passage no. 5 b) SCs at passage no. 4 FBS/Fsk/Nrg1 in DMEM	FBS in DMEM, 24h + Nrg1 (0, 15.625, 31.25, 62.5 pM) in DMEM, 2h	0, 15.625, 31.25, 62.5 pM Nrg1 +/- 80 µM Glu Positive Ctr: Nrg1 5nM 10 min	Baseline reached Glu decreases the effect of Nrg1, except only for the phosphorylation of AKT when cells were exposed to the higher concentrations of Nrg1 a) Phosphorylation of AKT, S6RP and ERK increases as higher concentrations of Nrg1 are added In the absence of Nrg1, Glu triggers the activation of AKT/S6RP and ERK pathways b) Phosphorylation of AKT, S6RP and ERK is not so robust and generally decreases as higher concentrations of Nrg1 are added In the absence of Nrg1, Glu triggers only the activation of ERK pathway	2
6	Test whether Glu enhances the effect of Nrg1 at higher concentrations than those tested in *Saitoh et al*. (2016) on a culture subconfluent as used in *Campana et al*. (2017)	~85% cell confluence a) SCs at passage no. 5 b) SCs at passage no. 4 FBS/Fsk/Nrg1 in DMEM	FBS in DMEM, 24h + Nrg1 (0, 0.1, 0.3, 1 nM) in DMEM, 2h	0, 0.1, 0.3, 1 nM Nrg1 +/- 80 µM Glu Positive Ctr: Nrg1 5nM 10 min	Baseline reached a) Phosphorylation of AKT, S6RP and ERK generally increases as higher concentrations of Nrg1 are added Glu decreases the effect of Nrg1, except only for the phosphorylation of AKT when cells were exposed to the lower concentration of Nrg1 Phosphorylation of AKT, S6RP and ERK is even lower when Glu alone is added than in the absence of stimuli b) Phosphorylation of AKT, S6RP and ERK is more robust and generally increases as higher concentrations of Nrg1 are added Glu generally decreases the effect of Nrg1 on the phosphorylation of ERK and S6RP Glu increases the effect of Nrg1 on the phosphorylation of AKT: more the concentration of Nrg1 more the phosphorylation is enhanced In the absence of Nrg1, Glu triggers only the phosphorylation of S6RP	2

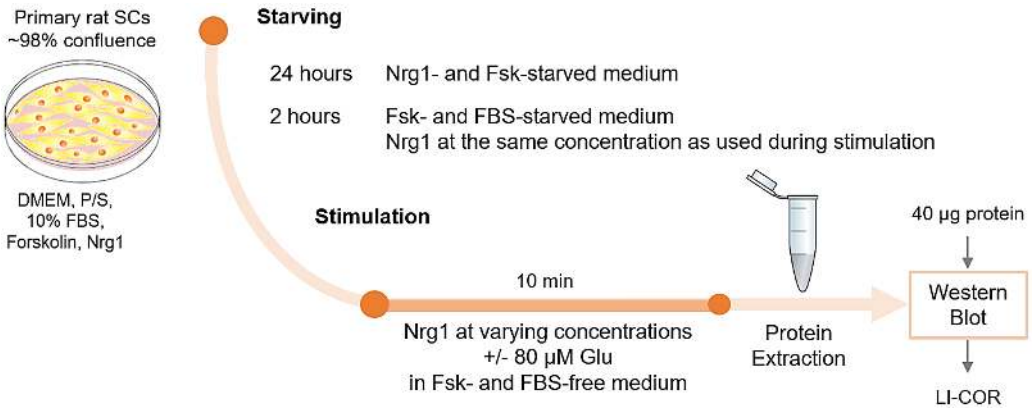

Figure 7. Scheme of the protocol to test whether ionotropic glutamate signaling in confluent cultured SCs modulates Nrg1-induced activation of AKT/S6RP and ERK subcellular signaling.

A

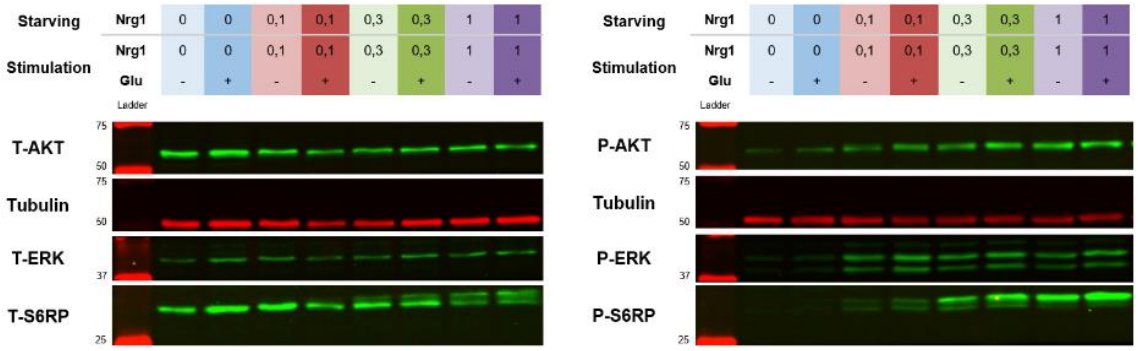

B

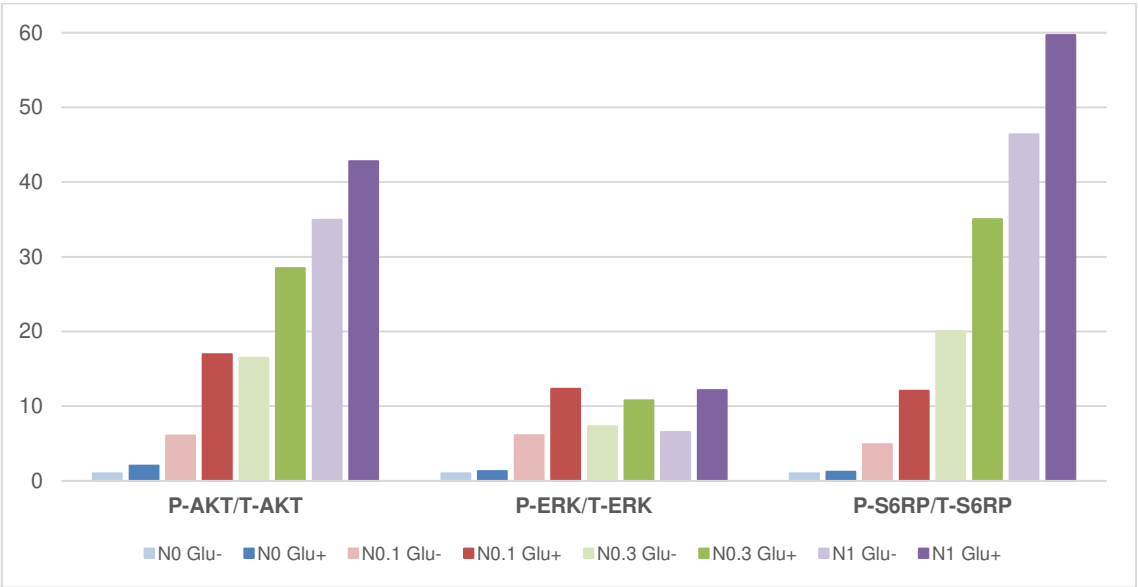

Figure 8. Immunoblot images (**A**) and quantified expression levels (**B**) of phosphorylated/total AKT, ERK, and S6RP in primary cultured SC after treatment for 10 min with Glu and Nrg1 at varying concentrations as indicated. The quantified expression level was normalized to the total protein expression level, relative to the condition without Nrg1 nor Glu (n = 1).

Other features that may be underlying the variability of the results during the process of optimization include the varying volume of protein lysate loaded into the gel of Western blot among different samples. Even if the mass of protein loaded is always normalized, the volume of SDS – used to give all proteins present a uniform negative charge – is proportional to the volume of the protein lysate. The migration of the negatively-charged proteins to the positively charged electrode through the acrylamide gel, as well as the transfer of proteins from within the gel onto the nitrocellulose membrane to be targeted by antibodies, are more or less efficient according to the amount of SDS present (Kurien & Scofield, 2009). Occasionally in some assays, the volume of protein loaded differed perceptibly among conditions. After the quantification, normalization to the housekeeping protein and to the total protein may be insufficient to normalize the quality of the signal emitted among the different lanes, due to the fact that antibody detection efficacy is unevenly reliant on the amount of protein present in the membrane.

3.1.2. Monitoring fluctuations of the intracellular levels of lactate in cultured SCs in response to glutamate

According to our hypothesis, glutamate may trigger an increased lactate import and/or production in SCs, leading to a raise in intracellular lactate concentration. The increase in lactate is then accompanied by its release into the extracellular space, which stabilizes the levels of lactate inside the cell. Complementary processes would be expected to occur in neurons, leading to a peak of the lactate level soon after its uptake from the periaxonal space and before its consumption by oxidative metabolism to produce energy.

The global scenario is that the intracellular concentration of lactate varies according to its relative exchange between extracellular, cytosolic and mitochondrial compartments – corresponding respectively to the lactate/pyruvate import/export through MCTs, glycolytic production, and consumption through the TCA cycle. These intercellular and subcellular lactate shuttles move continuously toward a metabolic equilibrium (San Martín et al., 2013).

Laconic, a genetically-encoded FRET-based lactate sensor, can be a very useful tool for monitoring the dynamic changes in intracellular concentrations of lactate in real-time and at a single cell resolution (San Martín et al., 2013). Laconic is composed of two fluorescent reporter proteins – mTFP and Venus – flanking a bacterial protein complex termed LldR (**Figure 9**). The latter is formed by a lactate-binding/regulatory element and a DNA-binding domain (San Martín et al., 2013).

Even though the reporter proteins are expected to exhibit distinct peaks of fluorescence (492 nm for mTFP and 526 nm for Venus), the emission spectrum of the donor fluorophore mTFP overlaps with the excitation spectrum of the acceptor Venus. This enables mTFP-to-Venus transfer of energy to occur. When lactate binds to the sensor moiety, this domain undergoes conformational alterations, which in turn change the relative distance and/or orientation of mTFP and Venus, decreasing FRET efficiency (**Figure 9**). Thus, the change in FRET, which is simply measured by the relative light intensities emitted from the two fluorophores, correlates negatively with the change in lactate concentration (Hou et al., 2011; San Martín et al., 2013).

In the first place, our approach relied on trying to replicate the methodology reported by San Martín et al. (2013) to become acquainted with this novel tool as well as to optimize the parameters for our own system. Initially, we used HEK293T cells due to their low endogenous capacity to uptake glucose (Takanaga & Frommer, 2010), besides their fast growth and propensity for transfection.

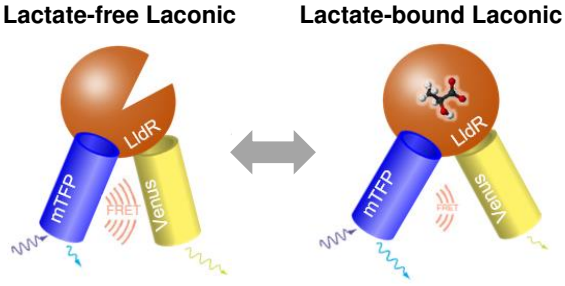

Figure 9. The reversible binding of lactate to Laconic decreases FRET efficiency. Adapted from (Hou et al., 2011; San Martín et al., 2013)

The overall procedure comprises transfecting subconfluent HEK293T cells with a plasmid encoding Laconic; setting up the FRET imaging system; exposing cells to media with a defined composition while acquiring over time the signals emitted by the two fluorophores; and processing the data (San Martín et al., 2013).

The first observation at the microscope was a clear fluorescence emitted by transfected HEK293 cells, specifically from the cytosol and not from the nucleus, as expected (San Martín et al., 2013). This shows that they were successfully lipofected with Laconic.

We then tested the effects of exposing our sample to different solutions: 5 mM glucose, 6 mM sodium oxamate, 10 mM lactate, 5 mM glucose + 10 mM lactate, and 5 mM glucose + 10 mM lactate + 1 µM AR-C155858 (ARC), all diluted in KRH (pH=7.4) buffer. All conditions could be tested on the same cells because we used a continuous superfusion system. Each condition was tested during 5 minutes to guarantee the steady-state to be reached.

The experiment began by exposing cultured cells to 5 mM glucose in KRH HEPES pH7.4 buffer, our reference solution. Glucose is expected to be taken up and consumed by the cells to produce lactate by glycolysis, which is exported through MCTs (**Figure 10B**, point 1). After setting up the sample in our imaging system and allowing time for cells to reach the thermodynamic equilibrium under this condition, we initiated data acquisition. The mTFP/Venus ratio for the first signals detected was used to normalize all the following values. This way, the graph in **Figure 10A** represents the variation of mTFP/Venus, an estimate of the intracellular levels of lactate, in response to a metabolic stimulation compared to the steady-state condition in which glucose is available in the medium.

It is important to highlight that mTFP/Venus ratio is not a direct readout of lactate concentrations, which would require sensor calibration in each cell. Thus, since mTFP/Venus ratio values are not absolute, it is not appropriate to display the data acquired from different experiments in the same plot. The graph in **Figure 10A** is representative and corresponds to one out of the three assays that we performed using the same experimental settings.

Then we applied the same buffer without glucose (and any other carbon sources) that functions as a washing solution. We expected to observe a partial reduction in the FRET ratio, which would be due to the discontinuation of lactate production (**Figure 10B**, point 2). However, we were unable to visualize clearly any variation of the signal.

After re-exposing the cells to reference solution, they were exposed to 6 mM sodium oxamate to pump out any residual lactate. Oxamate is a non-metabolizable substrate of MCTs and inhibitor of LDH, with a fast and reversible mode of action (Yang et al., 2014). When oxamate is transported by MCTs, it produces a trans-acceleration-exchange, pumping lactate to the extracellular space (Brown & Brooks, 1994) (**Figure 10B**, point 3). With this procedure, no lactate is presumably present inside the cell, and, consequently, we obtained the minimum value of mTFP/Venus ratio (Rmin).

Cells were exposed again to the reference buffer in order to return to the original baseline. Following a washing step, we activated the perfusion of 10 mM lactate, which is supposed to enter in the cell at a high rate due to the difference of concentrations on each side of the plasma

membrane (**Figure 10B**, point 4). At a certain point, the saturation of the transporters is achieved. Indeed, the mTFP/Venus ratio increased substantially upon exposure to lactate and then stabilized.

In order to reach the maximum value of mTFP/Venus ratio (Rmax) for this experiment, we loaded the cells with lactate up to Laconic saturation. For that end, we gave another pulse of 10 mM lactate but in the presence of 5 mM glucose. This way, the intracellular lactate can rise through glycolysis and import of extracellular lactate (**Figure 10B**, point 5). The additional presence of 1 µM of ARC in the medium blocks the exit of lactate, since ARC is an inhibitor of MCT1 and MCT2 (Ovens et al., 2010). Glycolytic lactate production further enhances lactate accumulation, resulting in the full sensor saturation, this is Rmax (**Figure 10B**, point 6). Since 10 mM is already very close to Laconic saturation, a substantial change in FRET ratio in the presence of glucose and ARC was not observed.

The outcome from this test showed some imperfections. Specifically, the signal was very weak, which gave rise to the noisy traces in the mTFP/Venus ratio plot. Since the nanosensor is ratiometric, potential artifacts induced by volume or focus changes are canceled out by the mTFP/Venus ratio (San Martín et al., 2013). Thus, the low signal intensity may be due to low expression of the sensor by the cells. Indeed, we specifically selected cells with low signal intensity to avoid saturation of the detector. As such, we propose optimizing the step of HEK293T cells transfection with Laconic for the future experiments, as well as adjusting the laser intensity to avoid saturation and bleaching. Moreover, cell-to-cell variability can naturally occur, even if this parameter was always taken into account when the regions of interest for signal acquisition were defined.

The results can be analyzed in a relative or absolute manner. For relative quantification, a simple comparison of the steady-state FRET ratio before/after exposure to a stimulus is suitable. For absolute quantification of intracellular lactate concentrations, a quadratic equation can be used based on the Rmin, Rmax and K_D constants for Laconic determined *in vitro* (San Martín et al. 2013).

In order to apply this system to SCs and perform an absolute quantification, we must confirm that Laconic behaves in a similar way in a different cell type. That would require an invasive calibration protocol with cellular permeabilization to determine if the K_D values vary (San Martín et al., 2013). However, this is not necessary for the relative quantification approach. For our purposes, the comparison of FRET ratios before and after exposure to glutamate, for example, should be adequate and sufficiently informative. One point to take into account is that SCs also express MCT4, which is not inhibited by ARC. In this case, we will have to combine ARC with the irreversible inhibitor pCMBS (4-(chloromercuri)benzenesulfonic acid sodium salt), a modifier of SH groups in proteins (Zhang & Solomon, 1992). Alternatively, the expression of a given MCT type in cultured SCs could be knocked-down using, for instance, shRNA, and Laconic could then be used to assess the contribution of specific isoforms to flux of lactate.

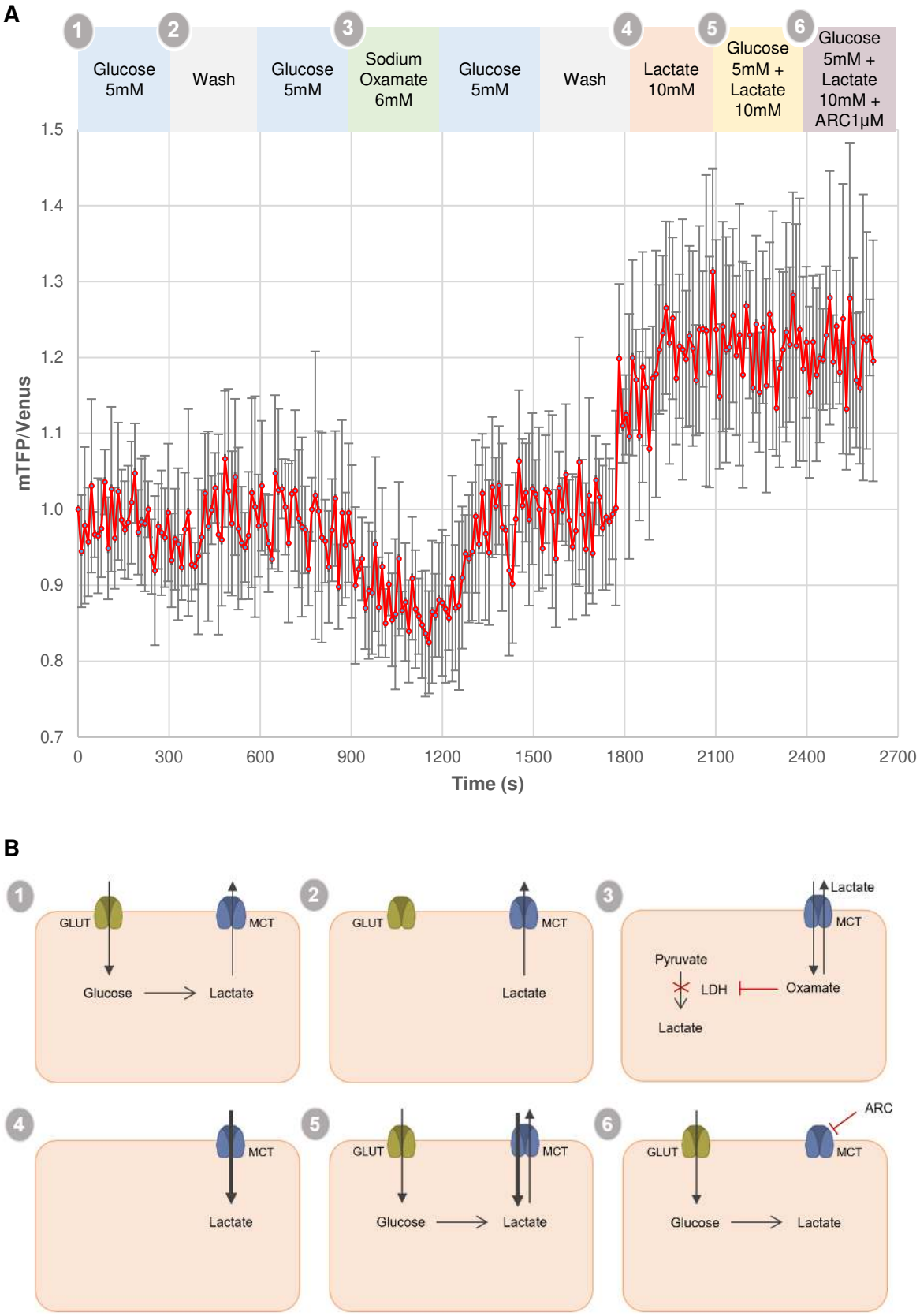

Figure 10. A. Graph showing the variations on the mTFP/Venus intensity upon exposing HEK293T cells to the indicated conditions over time. The bars represent the standard deviation (n = 3 or 5 cells).
B. Schematic representation of the expected cellular responses developed under the conditions numbered above the graph.

3.2. Characterization of *in vivo* models to study the role of MCTs in SCs

Myelinating SCs and neurons in the PNS were reported to express monocarboxylate transporters (Domènech-Estévez et al., 2015). This evidence was crucial for the formulation of our hypothesis. MCT1 and MCT4 were mainly found in regions of non-compacted myelin, potentially to serve as a route by which SCs provide lactate to the underlying axon (Domènech-Estévez et al., 2015).

In order to explore the neuron-glial metabolic communication in the PNS, and particularly to disclose the role of peripheral MCTs *in vivo*, we proposed to characterize the phenotype of cKO mouse models where MCT1 or MCT4 were specifically ablated in SCs.

MCT1 cKO mice carry the exon 5 flanked with LoxP sites in both alleles of *mSLC16A1* gene (coding for MCT1). In MCT4 cKO mice, in turn, the exons 3, 4 and 5 in both alleles of *mSLC16A3* gene (coding for MCT4) are flanked with LoxP sites. In opposition to the respective control animals, MCT1 or MCT4 cKO animals further carry Cre recombinase under the promoter of myelin protein zero (P0), which is specifically activated in SCs between embryonic days 13.5 and 14.5 (M. A. Feltri et al., 1999) (**Figure 11**).

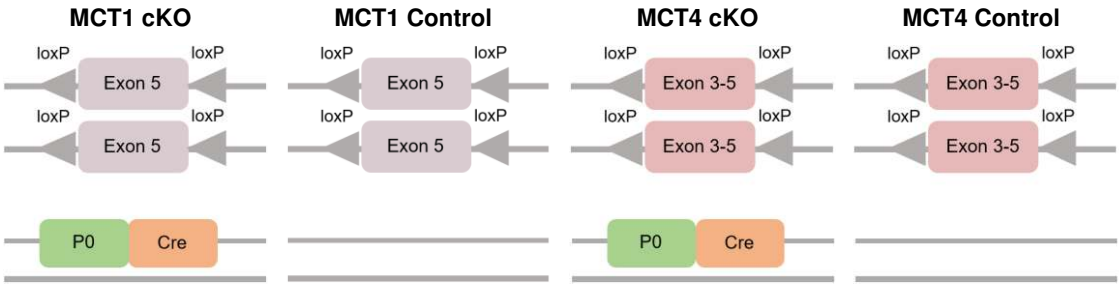

Figure 11. Schematic representation of the mutations carried by homozygous cKO mice for MCT1 and MCT4, and respective control animals.

We first performed analysis at the DNA, RNA and protein levels to evaluate the specificity and efficiency of MCT1 or MCT4 depletion. Conditional knock-out and control mice were compared at those levels respectively by means of genotyping, q-PCR using RNA extracted from the endoneurium of sciatic nerves (SN), and immunohistochemistry on both teased fibers and cross sections of sciatic nerves.

Once the animal models started to be validated, we analyzed the consequences of the loss of MCT1 and MCT4 in SCs in these animals by assessing the integrity of the neuromuscular junctions and the density of sensory innervation.

3.2.1. Validation of the mouse models

Genotyping

Genotyping PCR was indispensable during the process of generation of homozygous cKO mice and mouse line expansion, and always used to confirm the genotype of the animals before collecting their tissues/cells for analysis.

Using primers that target the LoxP site we were able to distinguish homozygous (1 flox band), heterozygous (1 flox band + 1 WT band) and WT (1 WT band) animals for the insertion of floxed exons of *mSLC16A1* or *mSLC16A3*. To distinguish cKO from control mice, a pair of primers specific for Cre recombinase was used in combination with primers targeting the gene encoding for IL-2 in mouse, which was used only to confirm the presence of DNA.

After extracting DNA from a biopsy of ear or tail from each animal, the targeted sequences of DNA were amplified by PCR and the products were separated by electrophoresis following the respective length (**Table 10**). **Figure 12** shows the electrophoretic profile of bands that are visualized for MCT1 Control, MCT1 cKO, MCT4 Control, and MCT4 cKO mice before Cre recombination.

Table 10. Expected length of the amplification products.

	Flox	WT
MCT1	227 bp	166 bp
MCT4	507 bp	446 bp
Cre	450 bp	
IL-2	327 bp	

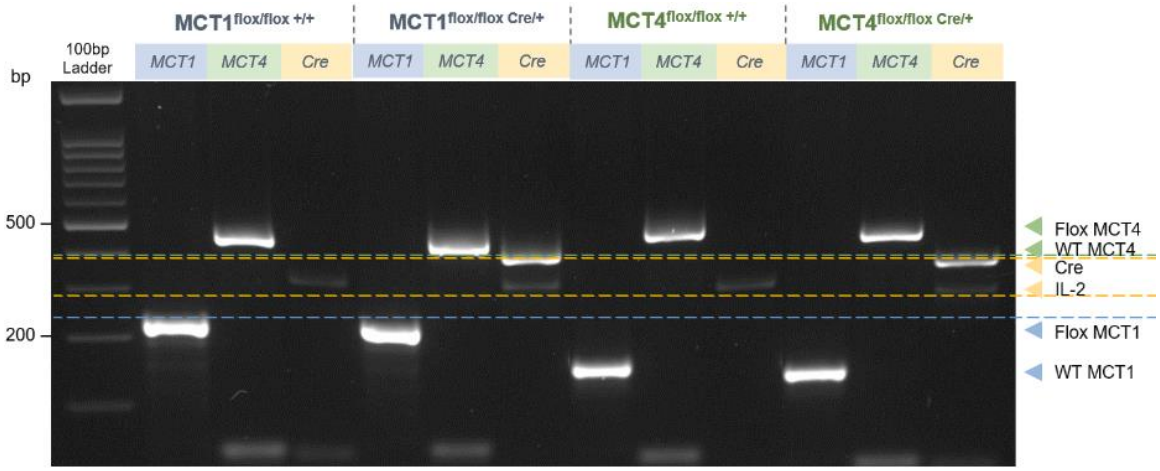

Figure 12. Electrophoretic separation of amplified segments of DNA to specifically genotype MCT1 or MCT4 cKO mice and the respective control animals.

Quantitative PCR

We next aimed to determine whether removing part of the gene encoding for MCT1 or MCT4 had resulted effectively in a loss of expression. To investigate this, we extracted RNA from the endoneurium of sciatic nerves collected from 4-months-old mice of both mouse lines. The endoneurium is almost exclusively composed by axons and SCs, the latter being the major source of the RNA by a large margin.

The amplitude of expression of MCT1, MCT2, and MCT4, which are the types of MCTs reported to be expressed by SCs (Domènech-Estévez et al., 2015), was then determined by qPCR. We also evaluated the expression of P0 and ubiquitin-conjugating enzyme E2 (Ubiq), the latter being the reference gene used to normalize all the other values (**Figure 13**). The mRNA expression levels from MCT1 cKO mice and MCT4 cKO mice are presented relative to the respective control animals.

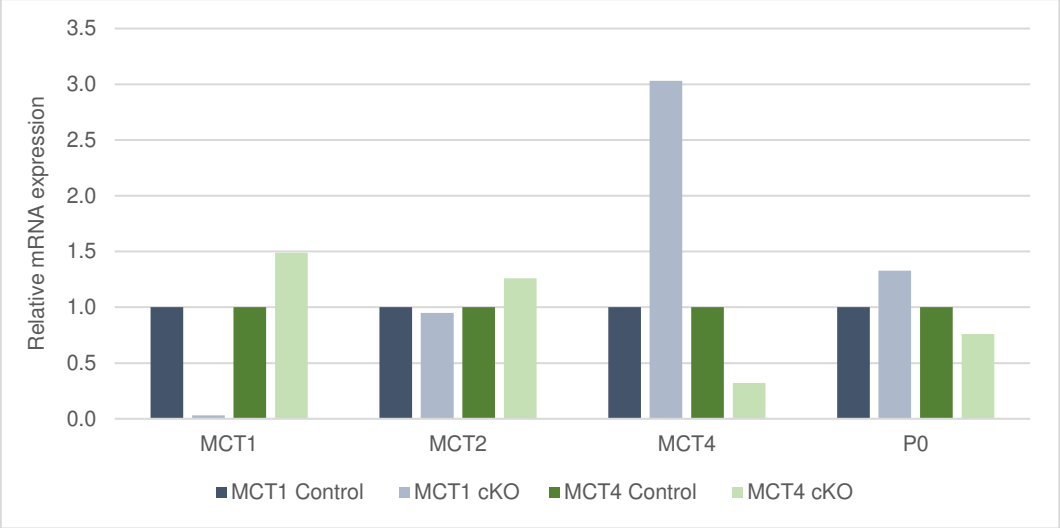

Figure 13. mRNA expression of MCT1, MCT2, MCT4 and P0 relative to the levels of Ubiq expression in sciatic nerve endoneurium of 4-months-old mice from both mouse lines (n = 1).

As expected, MCT1 cKO mice exhibited a strong decrease on the expression of MCT1 in comparison with the respective control. In the other mouse line, the depletion of MCT4 expression appeared to be less efficient. However, MCT4 expression in WT is low, therefore the qPCR efficiency may be interfering with the result. Of note, we observed that P0 was slightly less expressed in the MCT4 cKO animals compared to the MCT4 control mice, whereas the opposite effect was observed in the MCT1 cKO mouse line. Nevertheless, this quantitative analysis needs to be repeated with more samples, and it is required to perform studies at the level of mRNA translation into MCT1 or MCT4.

Interestingly, the depletion of MCT1 in SCs triggered a robust enhancement of MCT4 expression. In turn, MCT4 cKO mice exhibited higher expression of MCT1 and MCT2 when compared to the corresponding control. Therefore, this preliminary data points to a potential phenomenon of compensation activated in SCs for the loss of expression of MCT1 or MCT4.

Immunohistochemistry

Following gene transcription and RNA processing, additional regulatory processes can act to determine if – and at what extent – the expression of a given gene is translated into a functional protein (Cooper, 2000). For instance, miRNAs can modulate the RNA stability, which affects its lifetime and, consequently, the number of proteins produced (Cooper, 2000).

Having this in mind, we further studied the expression of MCT1 and MCT4 in the respective cKO and control mice at the protein level.

Immunostaining on teased fibers of sciatic nerves from adult mice of both lines revealed an efficient depletion of the respective isoform of MCT in the cKO animals. Whereas MCT1 unsurprisingly co-localized with phalloidin in MCT1 control mice (Domènech-Estévez et al., 2015), no MCT1 staining was observed in the cKO teased fibers, showing its efficient depletion from Schmidt-Lanterman incisures (SLIs) (**Figure 14**). In turn, MCT4 expression seems to be strongly decreased (or even absent) in the perinuclear cytoplasm of myelinating SCs (Domènech-Estévez et al., 2015) in the MCT4 cKO teased fibers (**Figure 15**). However, co-immunostaining against MCT4 and NF200 in cross sections of the MCT4 cKO sciatic nerve revealed the presence, although potentially reduced, of MCT4 in the perinuclear cytoplasm of SCs (**Figure 16**). Quantification of the MCT4 staining needs to be performed to compare the protein levels between the MCT4 cKO mice and the respective control. The validation of this mouse model is strictly dependent on the efficiency of MCT4 depletion.

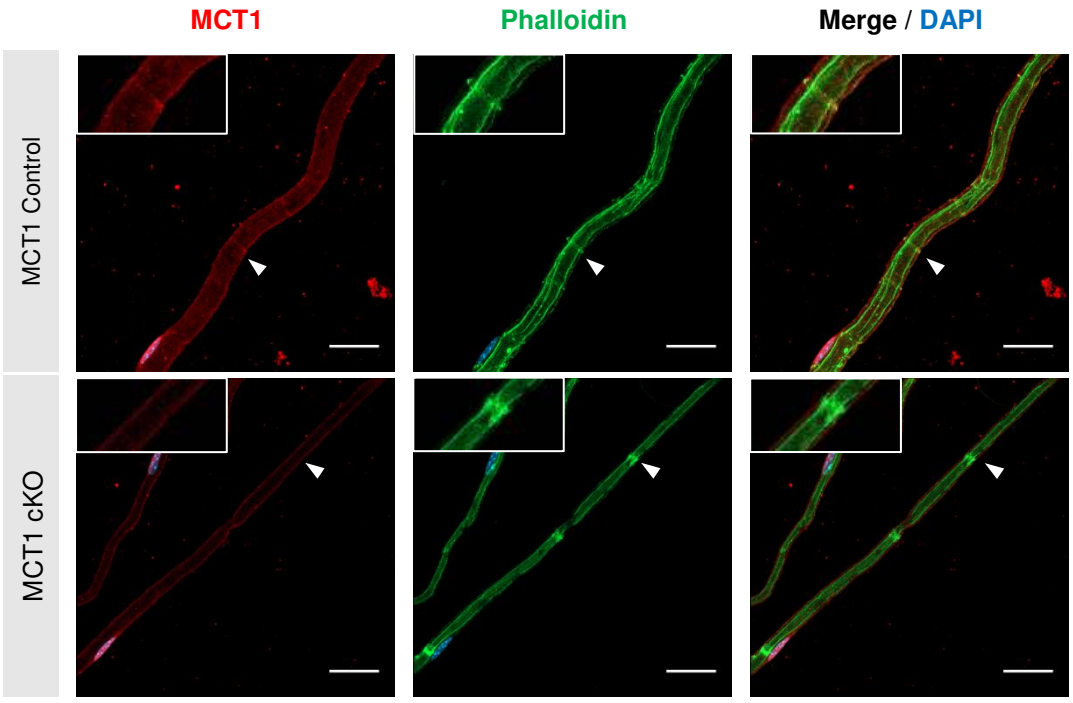

Figure 14. Co-immunostaining of MCT1/Phalloidin/DAPI on teased fibers prepared from sciatic nerves of adult MCT1 control and MCT1 cKO animals. Scale bar: 25µm

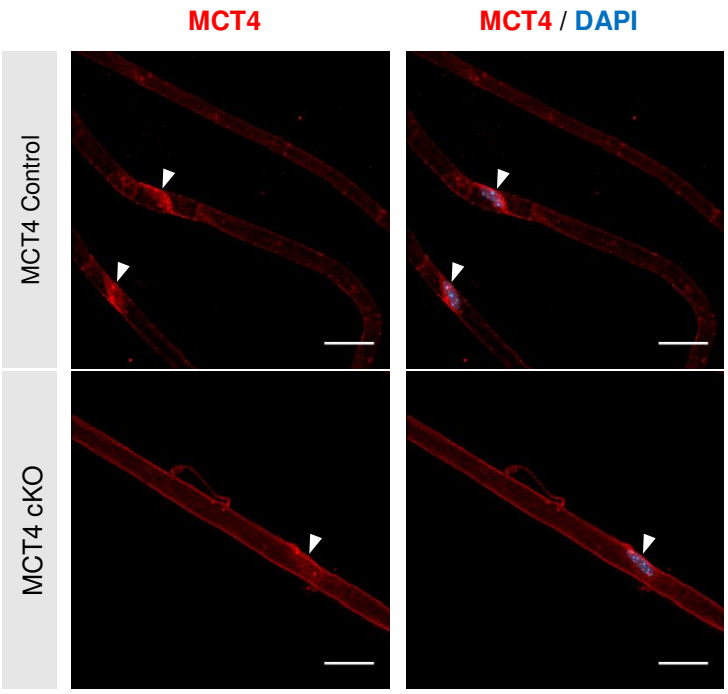

Figure 15. Immunostaining of MCT4 on teased fibers prepared from sciatic nerves of adult MCT4 control and MCT4 cKO animals. Scale bar: 25µm

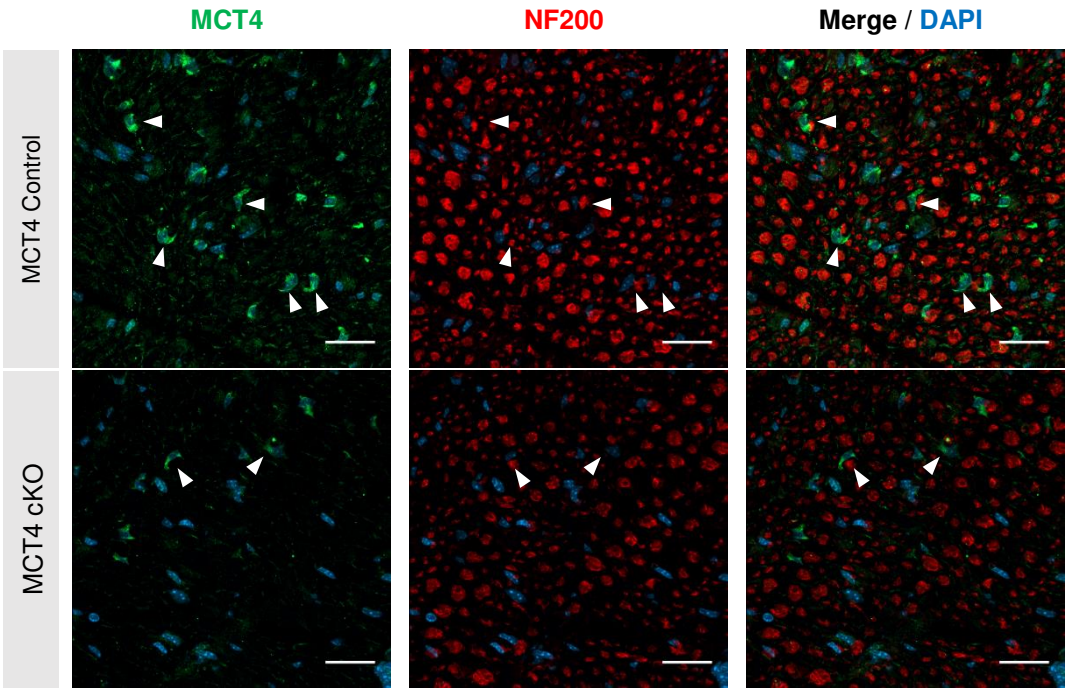

Figure 16. Co-immunostaining of MCT4/NF200/DAPI on cross sections of sciatic nerves from adult MCT4 control and MCT4 cKO animals. Scale bar: 25µm

Altogether, these experiments suggest that MCT1 cKO animals exhibit an efficient depletion of MCT1, as confirmed at the RNA and protein levels, which may be counteracted by an overexpression of MCT4. Regarding MCT4 cKO mice, the mRNA expression for MCT4 did not decrease as robustly, which was also reflected at the protein level.

3.2.2. Analysis of the effects of MCT1 or MCT4 depletion in the PNS

The consequences of the loss of MCT1 or MCT4 in SCs were previously assessed regarding the structure of myelinated fibers in sciatic nerves from both mouse models (data not shown). Myelin sheath thickness in function of the axonal diameter was determined by g-ratio measurements in semi-thin sections of sciatic nerve. Myelin ultrastructure and the density of myelinated fibers/Remak bundles were also evaluated by means of electron microscopy. No apparent differences were observed between MCT1 or MCT4 cKO mice and the respective control mice, neither at late development nor during adulthood. This data indicates that MCT depletion does not directly cause demyelination or myelin-related effects on peripheral nerves. This is not completely surprising, since peripheral neuropathies like CMT2, which are very debilitating, are also not associated with enlarged or hypertrophic peripheral nerves and exhibit slowly progressive weakness of distal muscles and mild or no sensory loss (Barreto et al., 2016).

To dissect whether MCT1 depletion in SCs affects the sensory or motor functions of peripheral fibers, we proposed to evaluate the intraepidermal nerve fiber density (IENFD) and the muscular innervation, respectively, on 1-year-old animals. Regarding the former, we immunostained sections of hind paw skin from two MCT1 cKO mice and one control animal for PGP9.5, a marker of sensory fibers (Mccarthy et al., 1995). DAPI staining was used to define the separation between dermis and epidermis based on the density of nuclei – keratinocyte nuclei in the epidermis are more compacted, while fibroblasts in the dermis are more spread in the collagenous matrix (**Figure 17**) (Mccarthy et al., 1995). So far, the preliminary quantification of intraepidermal PGP9.5-positive fibers normalized to the length of dermal-epidermal transition did not reveal significant differences between the cKO animals and the control. A reliable and statistically significant analysis requires the use of more animals. IENFD is also going to be determined for the MCT4 cKO mouse line.

To assess the impact of MCT depletion on motor functions of the PNS, we intended to measure the level of innervation in four different muscles (gastrocnemius, tibialis, soleus, and extensor digitorum longus) from 1-year-old animals. Neuromuscular junctions (NMJs), the expanded terminals formed when motor neuron axons synapse on skeletal muscles, express acetylcholine receptors that can be targeted by α-bungarotoxin (Herbst et al., 2010). Thus, the co-localization of the fluorescently labeled α-bungarotoxin with a neuronal marker, such as neurofilament, or a synaptic vesical marker indicates the extent of innervation. In **Figure 18**, we show an example of a fully innervated NMJs in a control animal.

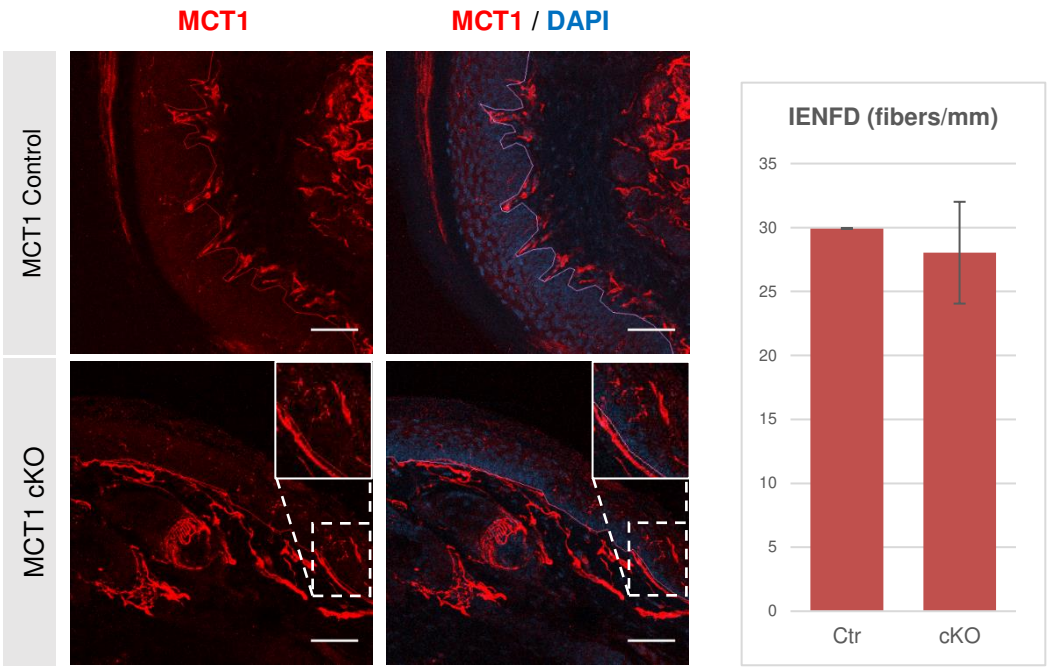

Figure 17. Immunostaining of mouse hindpaw skin to show intraepidermal nerve fibers (PGP9.5, red) and dermal-epidermal transition (traced line). Scale bar: 50µm. Quantification of IENFD in control (n = 1) and MCT1 cKO (n = 2) mice on the right. Scale bar represents the standard error of the mean.

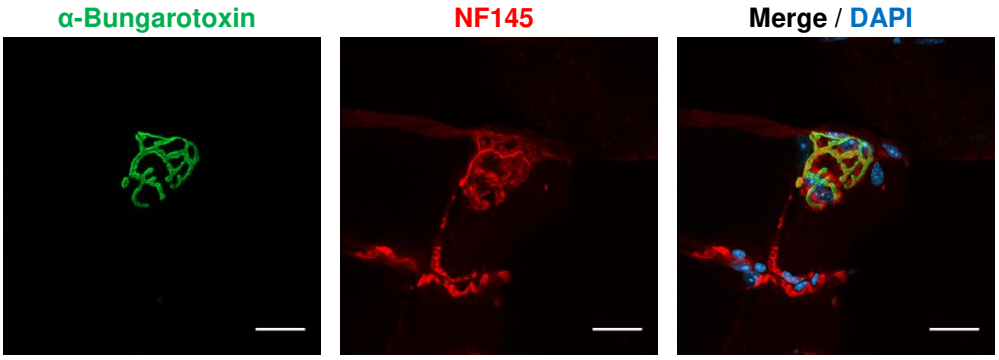

Figure 18. Co-localization of the α-bungarotoxin (green) with neurofilament-145 (NF145; red) showing a fully innervated neuromuscular junction in gastrocnemius muscle of MCT1 control animal. Scale bar: 25µm.

4. Conclusion and Future Perspectives

In conclusion, our data indicates that short-term *in vitro* exposure to glutamate signals via ionotropic receptors of confluent mature SCs to boost Nrg1/ErbB-mediated activation of AKT/S6RP and ERK pathways. Since these pathways can be involved in mobilization of energetic reserves, among others, these results support our initial hypothesis. Glutamate extrasynaptically released during axonal activity may trigger a metabolic shift in SCs towards increased production and release of lactate to properly support axons with energy substrates.

These data need to be confirmed with more assays in order to combine glutamate stimulation with FRET-based lactate measurements.

Additionally, we observed that SC-specific depletion of either MCT1 or MCT4 does not seem to perturb PNS structure and function, which could be due to a compensatory expression of other transporters. In order to understand this, we are establishing a MCT1/MCT4 double cKO and MCT2 cKO mouse lines to further explore the role of MCTs in the PNS.

As part of the characterization of these models, we are performing motor nerve conduction velocity measurements and will evaluate sensory and motor functions *in vivo* with behavioral tests (hot/cold plate, Von Frey filaments, rotarod, grip strength test, among others).

In the future, it would also be interesting to study the influence of MCTs in models of neuropathic disorders, such as ALS and CMT4C. This could give us some deeper understanding of the pathophysiology of these conditions, which could allow the development of new therapeutic strategies.

5. References

Amaral, A. I., Meisingset, T. W., Kotter, M. R., Sonnewald, U. (2013). Metabolic aspects of Neuron-Oligodendrocyte-Astrocyte interactions, *Frontiers in Endocrinology*, 4(54), 1–6. http://doi.org/10.3389/fendo.2013.00054

Balice-Gordon, R. J., Bone, L. J., & Scherer, S. S. (1998). Functional Gap Junctions in the Schwann Cell Myelin Sheath. *The Journal of Cell Biology*, 142(4), 1095–1104.

Barreto, L.C.L.S., Oliveira, F.S., Nunes, P.S., de França Costa, I.M.P., Garcez, C.A., Goes, G.M., Neves, E.L.A., de Souza Siqueira Quintans J., de Souza Araújo A.A. (2016). Epidemiologic Study of Charcot-Marie- Tooth Disease : A Systematic Review, *Neuro-epidemiology*, 46(3), 157–165. http://doi.org/10.1159/000443706

Barros, L. F. (2013). Metabolic signaling by lactate in the brain. *Trends in Neurosciences*, 36(7), 396–404. http://doi.org/10.1016/j.tins.2013.04.002

Beirowski, B. (2013). Concepts for regulation of axon integrity by enwrapping glia. *Frontreirs in Cellular Neuroscience,* 7(256), 1–22. http://doi.org/10.3389/fncel.2013.00256

Beirowski, B., Babetto, E., Golden, J. P., Chen, Y., Yang, K., Gross, R. W., … Milbrandt, J. (2014). Metabolic regulator LKB1 plays a crucial role in Schwann cell-mediated axon maintenance. *Nature Neuroscience*, 17(10), 1351–1361. http://doi.org/10.1038/nn.3809

Bergersen, L., Wærhaug, O., Helm, J., Thomas, M., Laake, P., Davies, A. J., … Ottersen, O. P. (2001). A novel postsynaptic density protein : the monocarboxylate transporter MCT2 is co-localized with δ -glutamate receptors in postsynaptic densities of parallel fiber – Purkinje cell synapses, 1, 523–534. http://doi.org/10.1007/s002210000600

Bhaskar, P. Hay, N. (2007). Review The Two TORCs and Akt. *Developmental Cell*, 12, 487–502. http://doi.org/10.1016/j.devcel.2007.03.020

Bishop, M. J., Everse, J., Kaplan, N. (1972). Identification of Lactate Dehydrogenase Isoenzymes by Rapid Kinetics. *PNAS,* 69(7), 1761–1765.

Brinkmann, B. G., Agarwal, A., Sereda, M. W., Garratt, A. N., Mu, T., Wende, H., … Nave, K. A. (2008). Neuregulin-1 / ErbB Signaling Serves Distinct Functions in Myelination of the Peripheral and Central Nervous System. *Neuron*, 59(4), 581–595. http://doi.org/10.1016/j.neuron.2008.06.028

Brockes, J. P., Fields, K. L., & Raff, M. C. (1979). Studies on Cultured Rat Schwann Cells. I. Establishment of Purified Populations From Cultures of Peripheral Nerve. *Brain Research*, 165(1), 105–118. https://doi.org/10.1016/0006-8993(79)90048-9

Brown, A. M., Evans, R. D., Black, J., Ransom, B. R. (2012). Schwann cell glycogen selectively supports myelinated axon function. *ANNALS of Neurology*, *72*(3), 406–418. http://doi.org/ 10.1002/ana.23607

Brown, A. M., Ransom, B. R. (2007). Astrocyte glycogen and brain energy metabolism. *Glia*, *55*(12), 1263–1271. http://doi.org/10.1002/glia.20557

Brown, M. A., & Brooks, G. A. (1994). Trans-Stimulation of Lactate TRansport from Rat Sarcolemmal Membrane Vesicles. *Archives of Biochemistry and Biophysics*, 313(1), 22–28

Buttermore, E. D., Thaxton, C. L., Bhat, M. A., Carolina, N. (2013). Organization and Maintenance of Molecular Domains in Myelinated Axons. *Journal of Neuroscience Research*, 91(5), 603–622. http://doi.org/10.1002/jnr.23197

Campana, W. M., Mantuano, E., Azmoon, P., Henry, K., Banki, M. A., Kim, J. H., Pizzo, D. P., Gonias, S. L. (2017). Ionotropic glutamate receptors activate cell signaling in response to glutamate in Schwann cells, *The FASEB Journa*l, 31(4), 1744-1755. http://doi.org/10.1096/fj.201601121R

Ceci, M. L., Mardones-krsulovic, C., Sánchez, M., Valdivia, L. E., Allende, M. L. (2014). Axon-Schwann cell interactions during peripheral nerve regeneration in zebrafish larvae. *Neural Development*, 9(22), 1–21. http://doi.org/10.1186/1749-8104-9-22

Chen, S., Rio, C., Ji, R., Dikkes, P., Coggeshall, R. E., Woolf, C. J., Corfas, G. (2003). Disruption of ErbB receptor signaling in adult non-myelinating Schwann cells causes progressive sensory loss. *Nature Neuroscience*, *6*(11), 1186–1193. http://doi.org/10.1038/nn1139

Chih, C., Lipton, P., Roberts, E. L. (2001). Do active cerebral neurons really use lactate rather than glucose ? *Trends in Neurosciences*, *24*(10), 573–578. https://doi.org/10.1016/S0166-2236(00)01920-2

Cooper, G. M. (2000). The Cell: A Molecular Approach. 2nd edition. Sunderland (MA): Sinauer Associates.

Domènech-Estévez, E., Baloui, H., Repond, C., Rosafio, K., Médard, J.-J., Tricaud, N., … Chrast, R. (2015). Distribution of Monocarboxylate Transporters in the Peripheral Nervous System Suggests Putative Roles in Lactate Shuttling and Myelination. *The Journal of Neuroscience*, 35(10), 4151–4156. http://doi.org/10.1523/JNEUROSCI.3534-14.2015

Feltri, M. A., D'Antonio, M., Previtali, S., Fasolini, M., Messing, A., & Wrabetz, L. (1999). P0-Cre Transgenic Mice for Inactivation of Adhesion Molecules in Schwann Cells. *Ann N Y Acad Sci*, 883 (1), 116–123.

Feltri, M. L., Poitelon, Y., & Previtali, S. C. (2016). How Schwann cells sort axons: new concepts. *The Neuroscientist*, 22(3), 252-265. http://doi.org/10.1177/1073858415572361.

Ferri, A., Cozzolino, M., Crosio, C., Nencini, M., Casciati, A., Gralla, E. B., … Carri, M. T. (2006). Familial ALS-superoxide dismutases associate with mitochondria and shift their redox potentials. *PNAS*, 103(37), 13860–13865. https://doi.org/10.1073/pnas.0605814103

Frühbeis, C., Fröhlich, D., Kuo, W. P., Amphornrat, J., Thilemann, S., Saab, A. S., … Krämer-Albers, E.-M. (2013). Neurotransmitter-Triggered Transfer of Exosomes Mediates Oligodendrocyte – Neuron Communication. *PLoS One*, 11(7), 1–19. http://doi.org/10.1371/journal.pbio.1001604

Funfschilling, U., Supplie, L. M., Mahad, D., Boretius, S., Saab, A.S., Edgar, J., … Nave, K. (2013). Glycolytic oligodendrocytes maintain myelin and long-term axonal integrity, *Nature*, 485(7399), 517–521. http://doi.org/10.1038/nature11007.

Garbern, J. Y., Yool, D. A., Moore, G. J., Wilds, I. B., Faulk, M. W., Klugmann, M., … Griffiths, I. R. (2002). Patients lacking the major CNS myelin protein , proteolipid protein 1 , develop length-dependent axonal degeneration in the absence of demyelination and inflammation. *Brain*, 125(Pt3), 551–561. http://doi.org/10.1021/bi000464+

Griffin, J. W., Thompson, W. J. (2008). Biology and Pathology of Nonmyelinating Schwann Cells, *Glia*, 56(14), 1518–1531. http://doi.org/10.1002/glia.20778

Grollman, E. F., Philp, N. J., McPhie, P., Ward, R. D., & Sauer, B. (2000). Determination of transport kinetics of chick MCT3 monocarboxylate transporter from retinal pigment epithelium by expression in genetically modified yeast. *Biochemistry*, 39(31), 9351-9357

Halestrap, A. P. (2012). The monocarboxylate transporter family — structure and functional characterization. *IUBMB LIfe*, *64*(1), 1–9. http://doi.org/10.1002/iub.573

Harrisingh, M. C., Perez-nadales, E., Parkinson, D. B., Malcolm, D. S., Mudge, A. W., Lloyd, A. C. (2004). The Ras / Raf / ERK signalling pathway drives Schwann cell dedifferentiation, *The EMBO Journal*, 23(15), 3061–3071. http://doi.org/10.1038/sj.emboj.7600309

Herbst, R., Iskratsch, T., Unger, E., & Bittner, R. E. (2010). Aberrant Development of Neuromuscular Junctions in Glycosylation-Defective Largemyd Mice. *Neuromuscul Disord.*, 19(5), 366–378. http://doi.org/10.1016/j.nmd.2009.02.011.

Hildebrand, C., Remahl, S., Persson, H., Bjartmar, C. (1993). Myelinated nerve fibres in the CNS. *Progress in Neurobiology,* 40(3), 319-384. https://doi.org/10.1016/0301-0082(93)90015-K

Hirrlinger, J., Nave, K. (2014). Adapting Brain Metabolism to Myelination and Long-Range Signal Transduction. *Glia*, 62(11), 1749-61. http://doi.org/10.1002/glia.22737

Hou, B., Takanaga, H., Grossmann, G., Chen, L., Qu, X., Jones, A. M., … Frommer, W. B. (2011). Optical sensors for monitoring dynamic changes of intracellular metabolite levels in mammalian cells. *Nature Protocols*, 6(11), 1818–1833. http://doi.org/10.1038/nprot.2011.392

Hughes, R. A. C. (2002). Peripheral neuropathy. *BMJ*, 324(7335), 466–469. https://doi.org/10.1136/bmj.324.7335.466

Hui, S., Ghergurovich, J. M., Morscher, R. J., Jang, C., Teng, X., Lu, W., … Rabinowitz, J. D. (2017). Glucose feeds the TCA cycle via circulating lactate. *Nature*, *551*(7678), 115–118. http://doi.org/10.1038/nature24057

Jahn, O., Tenzer, S., Werner, H. B. (2009). Myelin Proteomics : Molecular Anatomy of an Insulating Sheath. *Molecular Neurobiology*, 40(1), 55–72. http://doi.org/10.1007/s12035-009-8071-2

Jensen, V. F., Mølck, A.M., Bøgh, I. B., Lykkesfeldt, J. (2014). Effect of Insulin-Induced hypoglycaemia on the peripheral nervous system : focus on adaptive mechanisms , pathogenesis and histopathological changes. *Journal of Neuroendocrinology,* 26(8), 482–496. http://doi.org/10.1111/jne.12170

Jessen, K. R. (2004). Glial cells. *The International Journal of Biochemistry & Cell Biology*, 36(10), 1861–1867. http://doi.org/10.1016/j.biocel.2004.02.023

Jessen, K. R., Mirsky, R. (2005). The origin and development of glial cells in peripheral nerves. *Nature Reviews Neuroscience*, 6, 671–682. http://doi.org/10.1038/nrn1746

Jessen, K. R., Mirsky, R. (1999). Schwann cells and their precursors emerge as major regulators of nerve development. *Trends in Neurosciences*, 22(9), 402-410, https://doi.org/10.1016/S0166-2236(98)01391-5.

Kandel, E. R., Schwartz, J. H.; Jessel, T. M. (2000). Principles of Neural Science. 4th Edition. New York: McGraw-Hill.

Kirschner, D. A., Ganser, A. L. (1980). Compact myelin exists in the absence of basic protein in the shiverer mutant mouse. *Nature*, 283, 207–210, doi:10.1038/283207a0

Kisner, C., Colby, L. A. (2012). Therapeutic exercise: foundations and techniques. 6th Edition. Retrieved from http://ebookcentral.proquest.com

Kurien, B. T., & Scofield, R. H. (2009). Protein blotting and detection. *Methods in Molecular Biology*, 536.

Lappe-Siefke, C., Goebbels, S., Gravel, M., Nicksch, E., Lee, J., Braun, P. E., … Nave, K. (2003). Disruption of Cnp1 uncouples oligodendroglial functions in axonal support and myelination. *Nature Genetics*, 33, 366–374. http://doi.org/10.1038/ng1095

Laura, F. M., Yannick, P., Carlo, P. S. (2016). How Schwann Cells Sort Axons: New Concepts. *Neuroscientist*, 22(3), 252–265. http://doi.org/10.1177/1073858415572361

Lee, Y., Morrison, B. M., Li, Y., Lengacher, S., Farah, M. H., Hoffman, P. N., … Rothstein, J. D. (2012). Oligodendroglia metabolically support axons and contribute to neurodegeneration. *Nature*, 487(7408), 443–448. http://doi.org/10.1038/nature11314

Li, C., Tropak, M. B., Gerlai, R., Clapoff, S., Abramow-Newerly, W., Trapp, B., … Roder, J. (1994). Myelination in the absence of myelinassociated glycoprotein. *Nature*, 369, 747–750.

Lyons, D. A., Pogoda, H., Voas, M. G., Woods, I. G., Diamond, B., Nix, R., … Talbot, W. S. (2005). erbb3 and erbb2 Are Essential for Schwann Cell Migration and Myelination in Zebrafish. *Current Biology*, 15(6), 513–524. http://doi.org/10.1016/j.cub.2005.02.030

Maher, F., Vannucci, S. J., Simpson, I. A. (1994). Glucose transporter proteins in brain. *The FASEB Journal*, 8, 1003–1011. http://doi.org/10.1096/fasebj.8.13.7926364

Marat, A. L., & Haucke, V. (2016). Phosphatidylinositol 3 -phosphates — at the interface between cell signalling and membrane traffic. *The EMBO Journal*, 35(6), 561–579. http://doi.org/10.15252/embj.201593564

Marinkovic, P., Reuter, M., Brill, M. S., Godinho, L., Kerschensteriner, M., & Misgeld, T. (2012). Axonal transport de fi cits and degeneration can evolve independently in mouse models of amyotrophic lateral sclerosis. *PNAS*, 109(11), 4296–4301. http://doi.org/10.1073/pnas.1200658109/

Mathews, S. T., Plaisance, E. P., & Kim, T. (2009). Imaging systems for westerns: chemiluminescence vs. infrared detection. *Methods Mol Biol.*, 536, 499–513. http://doi.org/10.1007/978-1-59745-542-8_51

Matsuda, W., Furuta, T., Nakamura, K. C., Hioki, H., Fujiyama, F., Arai, R., Kaneko, T. (2009). Single nigrostriatal dopaminergic neurons form widely spread and highly dense axonal arborizations in the neostriatum, *The Journal of Neuroscience*, 29(2), 444–453. http://doi.org/10.1523/JNEUROSCI.4029-08.2009

Mccarthy, B. G., Hsieh, S., Stocks, A., Hauer, P., Macko, C., Cornblath, D. R., … Mcarthur, J. C. (1995). Cutaneous innervation in sensory neuropathies: Evaluation by skin biopsy. *Neurology*, 45(10), 1848–1855.

Michailov, G. V., Sereda, M. W., Brinkmann, B. G., Fischer, T. M., Haug, B., Birchmeier, C., … Nave, K-A. (2004). Axonal Neuregulin-1 Regulates Myelin Sheath Thickness. *Science*, 304(5671), 700–703. http://doi.org/ 10.1126/science.1095862

Morrison, B. M., Lee, Y., & Rothstein, J. D. (2013). Oligodendroglia: metabolic supporters of axons. *Trends in Cell Biology*, 23(12), 644-651. http://doi.org/10.1016/j.tcb.2013.07.007

Morrison, S. J., White, P. M., Zock, C., Anderson, D. J. (1999). Prospective Identification, isolation by flow cytometry, and in vivo self-renewal of multipotent mammalian neural crest stem cells. *Cell*, 96(5), 737–749, https://doi.org/10.1016/S0092-8674(00)80583-8

Nave, K. (2010a). Myelination and support of axonal integrity by glia. *Nature*, 468(7321), 244-252. http://doi.org/10.1038/nature09614

Nave, K. (2010b). Myelination and the trophic support of long axons. N*ature Reviews Neuroscience*, 11(4), 275-83. http://doi.org/10.1038/nrn2797

Nave, K., Salzer, J. L. (2006). Axonal regulation of myelination by neuregulin 1. *Current Opinion in Neurobiology*, 16, 492–500. http://doi.org/10.1016/j.conb.2006.08.008

Nave, K., Werner, H. B. (2014). Myelination of the nervous system : mechanisms and functions, *Annual Review of Cell Developmental Biology*, 30, 503-533, http://doi.org/10.1146/annurev-cellbio-100913-013101

Ogata, T., Iijima, S., Hoshikawa, S., Miura, T., Yamamoto, S., Oda, H., Nakamura, K., Tanaka, S. (2004). Opposing Extracellular Signal-Regulated Kinase and Akt Pathways Control Schwann Cell Myelination. *Journal of Neuroscience*, 24(30), 6724–6732. http://doi.org/10.1523/JNEUROSCI.5520-03.2004

Ovens, M. J., Davies, A. J., Wilson, M. C., Murray, C. M., & Halestrap, A. P. (2010). AR-C155858 is a potent inhibitor of monocarboxylate transporters MCT1 and MCT2 that binds to an intracellular site involving transmembrane helices 7-10. *Biochemical Journal.*, 425(3), 523–530. http://doi.org/10.1042/BJ20091515

Patzig, J., Jahn, O., Tenzer, S., Wichert, S. P., de Monasterio-schrader, P., Rosfa, S., … Werner, H. B. (2011). Quantitative and integrative proteome analysis of peripheral nerve myelin identifies novel myelin proteins and candidate neuropathy loci. *Journal of Neuroscience*, 31(45), 16369–16386. http://doi.org/10.1523/JNEUROSCI.4016-11.2011

Pellerin, L. (2003). Lactate as a pivotal element in neuron – glia metabolic cooperation. *Neurochemistry International*, 43(4-5), 331–338. http://doi.org/10.1016/S0197-0186(03)00020-2

Pellerin, L., Magistretti, P. J. (1994). Glutamate uptake into astrocytes stimulates aerobic glycolysis : a mechanism coupling neuronal activity to glucose utilization. *PNAS*, 91(22), 10625–10629

Pellerin, L., Pellegri, G., Bittar, P. G., Charnay, Y., Martin, J., Stella, N., & Magistretti, P. J. (1998). Evidence Supporting the Existence of an Activity-Dependent Astrocyte-Neuron Lactate Shuttle. *Developmental Neuroscience*, *20*, 291–299. https://doi.org/10.1159/000017324

Perkinton, M. S., Ip, J. K., Wood, G. L., Crossthwaite, A. J., & Williams, R. J. (2002). Phosphatidylinositol 3-kinase is a central mediator of NMDA receptor signalling to MAP kinase (Erk1 / 2), Akt / PKB and CREB in striatal neurones. *Journal of Neurochemistry*, 80(2), 239–254. https://doi.org/10.1046/j.0022-3042.2001.00699.x

Readhead, C., Popko, B., Takahashi, N., Shine, H. D., Saavedra, S. R. A., Sidman, R. L., Hood, L. (1987). Expression of a myelin basic protein gene in transgenic shiverer mice: correction of the dysmyelinating phenotype. *Cell*, 48(4), 703–712. http://doi.org/10.1016/0092-8674(87)90248-0

Rinholm, J., Bergersen, L. H. (2012). The wrap that feeds neurons. *Nature*, 487(7408), 435-436. htpp://doi.org/10.1038/487435a

Rinholm, J. E., Bergersen, L. H. (2014). White matter lactate - Does it matter? *Neuroscience*, *276*, 109–116. http://doi.org/10.1016/j.neuroscience.2013.10.002

Rinholm, J. E., Hamilton, N. B., Kessaris, N., Richardson, W. D., Bergersen, L. H., Attwell, D. (2011). Regulation of oligodendrocyte development and myelination by glucose and lactate. *The Jounal of Neuroscience*, 31(2), 538–548. http://doi.org/10.1523/JNEUROSCI.3516-10.2011

Riva, N., Chaabane, L., Peviani, M., Ungaro, D., Domi, T., Dina, G., … Quattrini, A. (2014). Defining Peripheral Nervous System Dysfunction in the SOD-1 G93A Transgenic Rat Model of Amyotrophic Lateral Sclerosis. *J Neuropathol Exp Neurol*, 73(7), 658–670. http://doi.org/10.1097/NEN.0000000000000081

Saab, A. S., Tzvetanova, I. D., Nave, K. (2013). The role of myelin and oligodendrocytes in axonal energy metabolism. *Current Opinion in Neurobiology*, 23(8), 1–8. http://doi.org/10.1016/j.conb.2013.09.008

Saitoh, F., Wakatsuki, S., Tokunaga, S., Fujieda, H., & Araki, T. (2016). Glutamate signals through mGluR2 to control Schwann cell differentiation and proliferation. *Nature*, 6(29856), 1–14. http://doi.org/10.1038/srep29856

Salzer, J. L. (2003). Polarized domains of myelinated axons. *Neuron*, 40(2), 297–318. https://doi.org/10.1016/S0896-6273(03)00628-7

Samara, C., Poirot, O., Domènech-estévez, E., Chrast, R. (2013). Neuronal activity in the hub of extrasynaptic Schwann cell-axon interactions. *Frontiers in Cellular Neuroscience*, 7(228), 1-11. http://doi.org/10.3389/fncel.2013.00228

San Martín, A., Ceballo, S., Ruminot, I., Lerchundi, R., Frommer, W. B., & Barros, L. F. (2013). A Genetically Encoded FRET Lactate Sensor and Its Use To Detect the Warburg Effect in Single Cancer Cells. *PLoS One*, 8(2), 1–11. http://doi.org/10.1371/journal.pone.0057712

Sánchez-Abarca, L., Tabernero, A., Medina, M. (2001). Oligodendrocytes use lactate as a source of energy and as a, percursor of lipids, *Glia*, 36(3), 321–329. http://doi.org/10.1002/glia.1119

Saporta, M. A., & Shy, M. E. (2014). Inherited Peripheral Neuropathies. *Neurol Clin*, 31(2), 597–619. http://doi.org/10.1016/j.ncl.2013.01.009.

Scherer, S. S., Arroyo, E. J. (2002). Recent progress on the molecular organization of myelinated axons, *Journal of the peripheral nervous system*, 7(1), 1–12. http://doi-org/10.1046/j.1529-8027.2002.02001.x

Schindelin, J., Arganda-carreras, I., Frise, E., Kaynig, V., Pietzsch, T., Preibisch, S., … Cardona, A. (2012). Fiji - an Open Source platform for biological image analysis. *Nature Methods*,

9(7), 678-682. http://doi.org/10.1038/nmeth.2019.

Sherman, D. L., Brophy, P. J. (2005). Mechanisms of axon ensheathment and myelin growth. *Nature Review Neuroscience*, 6(9), 683–690. http://doi.org/10.1038/nrn1743

Spencer, P. S., Sabri, M. I., Schaumburg, H. H., Moore, C. L. (1978). Does a defect of energy metabolism in the nerve fiber underlie axonal degeneration in polyneuropathies? *ANNALS of Neurology*, 5(6), 501-507, http://doi.org/10.1002/ana.410050602

Stys, P. K. (2011). The axo-myelinic synapse. *Trends in Neurosciences*, 34(8), 393–400. http://doi.org/10.1016/j.tins.2011.06.004

Takanaga, H., & Frommer, W. B. (2010). Facilitative plasma membrane transporters function during ER transit. *The FASEB Journal*, 24(8), 2849-2858. http://doi.org/10.1096/fj.09-146472

Taveggia, C., Zanazzi, G., Petrylak, A., Yano, H., Rosenbluth, J., Einheber, S., … Salzer J.L. (2005). Neuregulin-1 type III determines the ensheathment fate of axons. *Neuron*, 47(5), 681–694. http://doi.org/10.1016/j.neuron.2005.08.017

Timmerman, V., Clowes, V. E., & Reid, E. (2013). Overlapping molecular pathological themes link Charcot – Marie – Tooth neuropathies and hereditary spastic paraplegias. *Experimental Neurology*, 246, 14–25. http://doi.org/10.1016/j.expneurol.2012.01.010

Twiss, J. L., Fainzilber, M. (2009). Ribosomes in axons – scrounging from the neighbors ? *Trends in Cell Biology*, 19(5), 236-243. http://doi.org/10.1016/j.tcb.2009.02.007

Verkhratsky, A., & Kirchhoff, F. (2007). NMDA Receptors in Glia. *The Neuroscientist*, 13(1), 28–37. http://doi.org/10.1177/1073858406294270

Viader, A., Golden, J. P., Baloh, R. H., Schmidt, R. E., Hunter, D. A., Milbrandt, J. (2011). Schwann cell mitochondrial metabolism supports long-term axonal survival and peripheral nerve function. *The Journal of Neuroscience*, *31*(28), 10128–10140. http://doi.org/10.1523/JNEUROSCI.0884-11.2011

Webster, H. D. (1971). The geometry of peripheral myelin sheaths during their formation and growth in rat sciatic nerves. *Journal of cell biology*, 48(2), 348-367. htpp://doi.org/10.1083/jcb.48.2.348

Yang, Y., Su, D., Zhao, L., Zhang, D., Xu, J., Wan, J., & Chen, M. (2014). Different effects of LDH-A inhibition by oxamate in non-small cell lung cancer cells. *Oncotarget*, 5(23), 11886-11896. http://doi.org/10.18632/oncotarget.2620

Yarden, Y., Sliwkowski, M. X. (2001). Untangling the ErbB signalling network. *Nature reviews: Molecular cell biology*, 2(2), 127-137. htpp://doi.org/10.1038/35052073

Yu, A. C., H., Drejer, J., Hertz, L., Schousboe, A. (1983). Pyruvate carboxylase activity in primary cultures of astrocytes and neurons. *Journal of neurochemistry*, 41(5), 1484–1487. htpp://doi.org/ 10.1111/j.1471-4159.1983.tb00849.x

Zanazzi, G., Einheber, S., Westreich, R., Hannocks, M., Bedell-Hogan, D., Marchionni, M. A., Salzer, J. L. (2001). Glial growth factor / neuregulin inhibits schwann cell myelination and induces demyelination. *Journal of cell biology*, 152(6), 1289–1300.

Zhang, Z., & Solomon, A. K. (1992). Effect of pCMBS on anion transport in human red cell membranes. *Biochimica et Biophysica Acta*, 1106(1), 31–39. https://doi.org/10.1016/0005-2736(92)90218-B

Zorick, T. S., & Lemke, G. (1996). Schwann cell differentiation. *Current Opinion in Cell Biology*, 8(6), 870-876. https://doi.org/10.1016/S0955-0674(96)80090-1